Master of Science in
Cultural Heritage Materials & Technologies

Department of History, Archaeology
& Cultural Resources Management
University of the Peloponnese

UNIVERSITY OF THE PELOPONNESE

DIMITRIS MITSOS

(R.N. 1012201502007)

DIPLOMA THESIS:

CHARACTERIZATION OF BLACK CRUST ON PENTELIC AND KARYSTOS MARBLE IDENTIFICATION OF POLLUTION SOURCES

SUPERVISING COMMITTEE:

Dr. Evangelos Gerasopoulos, National Observatory of Athens

Assoc. Prof. Nikolaos Zacharias, University of the Peloponnese

EXAMINATION COMMITTEE:

Dr. Evangelos Gerasopoulos, National Observatory of Athens

Assoc. Prof. Nikolaos Zacharias, University of the Peloponnese

Dr. Vasiliki Kantarelou, N.C.S.R. Demokritos

KALAMATA, 26 JANUARY 2017

“Non est ad astra mollis e terris via”

- Seneca

ABSTRACT

Samples of black crusts from the western façade of the Library of Hadrian (Athens) have been collected and investigated. A complete chemical and mineralogical characterization of the degradation products was conducted through optical microscopy (OM), scanning electron microscopy (SEM), X-ray fluorescence and micro X-ray fluorescence (XRF and μ-XRF), and μ-Raman spectroscopy, in order to detect pollution sources. The decay features present on the surface of the monument, consist of typical black crusts and an iron-rich aluminosilicate patina. The chemical composition of the crusts, the element distribution along the crust and the characterization of individual embedded particles could reveal groups of elements related to specific sources and related to each other. Three main typologies of particles could be identified: a) carbonaceous particles from diesel exhausts and domestic boilers, b) Si-rich particles from vehicular emissions and mineral dust, and c) metallic Ti-rich and Fe-rich particles from coal combustion and domestic heating, respectively. The main source of pollution was revealed to be traffic, with a clear fingerprint of the type and chronological development of anthropogenic pollutant deposition in the area of central Athens evident within the black crusts.

Key words: black crusts, air pollution, particulate matter, marble weathering

ACKNOWLEDGEMENTS

I would like to start by thanking the Ephorate of Antiquities of Athens for providing the samples under investigation and especially Mr. Sourlas, the archaeologist surveying the Library of Athens and the area of the Roman Agora in general, Mr. Daskalakis, Head of the Conservation Department of the Ephorate and Mr. Korosis and Mrs. Antonopoulou, conservators of the Ephorate, for helping with obtaining the samples.

My supervisor, Dr Evangelos Gerasopoulos from the National Observatory of Athens, showed great capacity in consulting me about how versatility, resourcefulness and integration can lead to a successful result in handling such a complex subject. His invaluable information on air pollution and help whenever a problem occurred, helped in keeping the goals of this study always clear.

Co-supervisor Assoc. Professor Nikolaos Zacharias set the initial motivation for this study, by enthusiastically responding to the proposed subject. His constant encouragement throughout the whole conduction of the dissertation was essential.

Dr. Vasiliki Kantarelou from NCSR Demokritos and member of the examination committee, provided the μ-XRF measurements and the quantification of the results, thus helping in a very important part of this study.

I would also like to give special thanks to Eleni Palamara, candidate Dr. of the University of Peloponnese, as her help, guidance, involvement and encouragement in almost all technical parts of this study was crucial.

Finally, I would like to thank all of my classmates for sharing such an excellent academic experience and my family for supporting every step I make.

LIST OF TABLES

Table **Page**

LIST OF FIGURES

Figure **Page**

TABLE OF CONTENTS

1. INTRODUCTION

Historic monuments act not only as single architectural works to be viewed by visitors, but also as reminders of the setting in which the monument was constructed. They are living evidences of civilizations and historic developments or events. Conservation and restoration of such makings is essential in order to safeguard them as both works of art and historical evidence (ICOMOS, 1965).

The decay of cultural heritage is a longstanding problem, due to the natural process of weathering with the passage of time. The industrial revolution, along with the rapid changes it brought to the social and economic life, led to a declining state of environmental conditions and air quality in urban areas, adding another important parameter to the deterioration processes. Energy generation, industry and traffic are the most important sources of air pollutants in cities, directly affecting Cultural Heritage (Brimblecombe, 2003; Ghedini, et al., 2011; Cassar, 2016). External surfaces of built heritage in urban environments, being more susceptible to atmospheric agents, give rise to concerns about their future state of preservation. The contribution of atmospheric pollutants to damage on built heritage has been long noticed (Schaffer, 1932), although extensive research on this subject begun a few decades later.

Concentrations of fine particles from diesel vehicles have rapidly increased in the 21st century, causing blackening of facades of important monuments (Brimblecombe, 2015). This is due to the capability of atmospheric pollutants to form compounds that are stable enough to reach the building surface through wet or dry deposition and interact with the building materials. Air pollution, especially when matched with preferable climatic conditions, can lead to a significant reduction of the lifespan of materials and coatings (Ivaskova, et al., 2015). Through the interactions taking place on the surface of the materials, pollution-derived compounds can transform and produce new minerals, often followed by structural degradation of various levels and color change (Bonazza, et al., 2005; Smith, et al., 2008; Ozga, et al., 2014).

One of the most common effects of pollution on carbonate building surfaces is the formation of black crust, through the synergistic action of sulfur and nitrogen oxides, particulate matter and rain pH. It appears as a dark coating, where gypsum aggregates fixate atmospheric particles (Cachier, et al., 2004; Sanjurjo-Sánchez & Alves, 2011). The degradation products are quite visible in the case of calcareous building materials, causing blackening of the surfaces and chemical and structural instability (Rodriguez-Navarro & Sebastian, 1996; Török, et al., 2010). The dark color is attributed to the accumulation of carbonaceous particles on the material surface (Moropoulou, et al., 1998; La Russa, et al., 2013; Perez-Monserrat, et al., 2016).

The effects of air pollution on Cultural Heritage have been the subject of numerous studies, with an increasing interest throughout the last two decades. Special attention has been given to the description of the morphology, type, chemical composition and mineralogy of black crusts (Moropoulou, et al., 1998; Fronteau, et al., 2010; Török, et al., 2010; La Russa, et al., 2013; Ozga, et al., 2013). Identification of pollution sources is another subject that has been dealt with exhaustive research from various scopes. Mineralogy, isotopic composition, major/trace elements and ion presence in black crusts have been successfully used as tools for revealing a pollution source (Maravelaki-Kalaitzaki & Biscontin, 1999; Sabbioni, et al., 2003; Prieto-Taboada, et al., 2013; Perez-Monserrat, et al., 2016).

In this study, the monument under investigation is the Library of Hadrian, located in the centre of Athens. Samples of black crust were collected from the western façade, where blackening and structural deterioration was quite visible. Sampling provided an opportunity for a complete chemical and mineralogical characterization of the black crust, through optical microscopy (OM), scanning electron microscopy (SEM), X-ray fluorescence and micro X-ray fluorescence (XRF and μ-XRF), and μ-Raman spectroscopy.

In Chapter 2, the theoretical context necessary for a better understanding of the subject is presented. Attention is paid to the characteristics of the monument, the materials under study and their interaction with pollutants, along with a brief description of the environmental conditions and air quality in the surrounding area. In Chapter 3, the sampling conditions are described, along with the aim of the methodology used and the technical details of the analytical procedure. In Chapter 4, the results of each analytical technique are given. In Chapter 5, discussion of the results and further data processing is presented. Finally, in Chapter 6, conclusions are made and further thoughts on future approach on the subject are expressed.

Apart from recognising the chemical composition and minerals formed in the matrix, highlighting of the trace elements present inside the crust body can give insight into the origin of the pollutants responsible for the surface deterioration**.** Characterization of the corrosion products on the surface of monuments and identification of the main pollutants actively participating in the deterioration cycle is essential. This type of data can provide an opportunity to evaluate the state of preservation of the external surface of a monument, devise future preventive conservation strategies, and estimate the effect of the whole pollutant emission inventory for a specific area.

2. THEORETICAL CONTEXT

2.a Historical and architectural characteristics of the monument

The Library of Hadrian is located in the Monastiraki area, in the center of Athens, on the north side of the Acropolis and adjacent to a large group of monuments belonging to the Roman Agora. It is accessible through a pedestrian street (Areos St) that views on the western façade of the monument (Fig. 1). It was constructed by the Roman Emperor Hadrian in AD 132, along with other works of improvement for the city of Athens. It was built to impress, storing important literary works and administrative documents and hosting philosophical schools. The Library was severely damaged during the Herulian invasion in AD 267. It was later repaired by the Praetorian Prefect of Illyricum, Herculius, in AD 407-412. In the Byzantine period, three churches were built in the centre of its court, chronologically superseding each other. The site was used as the seat of the Voevode (Governor) during the occupation of Greece by the Ottoman Empire, as barracks by King of Greece Otto in 1835, and later as a prison (Graindor, 1935; Shear Jr, 1981; Choremi-Spetsieri, 1995; Greek Ministry of Culture, 2012).

Fig. 1: The western façade of the Library of Hadrian (Raddato, 2014).

The Library has an unmistakable Roman character. It is related in appearance with the Roman Agora; the general architectural scheme and scale are similar, due to Hadrian's intentions to connect past works with the newly erected buildings. The complex of the Library was built on a rectangular plan (122 x 82 m), with its entrance on the west side of the building. Inside the complex was an open peristyle courtyard, with a decorative pool and a garden, surrounded by colonnades with 100 columns. A series of rooms were located at the eastern side of the building, where the books of the library were stored. The square library itself was located opposite the entrance on the eastern side, with a reading room on each side and a lecture hall (auditorium) at the wings. The whole exterior of the building consisted of plain poros blocks, about 10 meters in height, except from the columns with Corinthian plates, along the western façade, at each side of the entrance (Fig.2-3). Today, the only remains of the original building are the open courtyard, part of the entrance and the southern part of the western façade, with seven Corinthian columns (Sisson, 1929; Shear Jr, 1981; Boatwright, 1983; Choremi-Spetsieri, 1995; Greek Ministry of Culture, 2012).

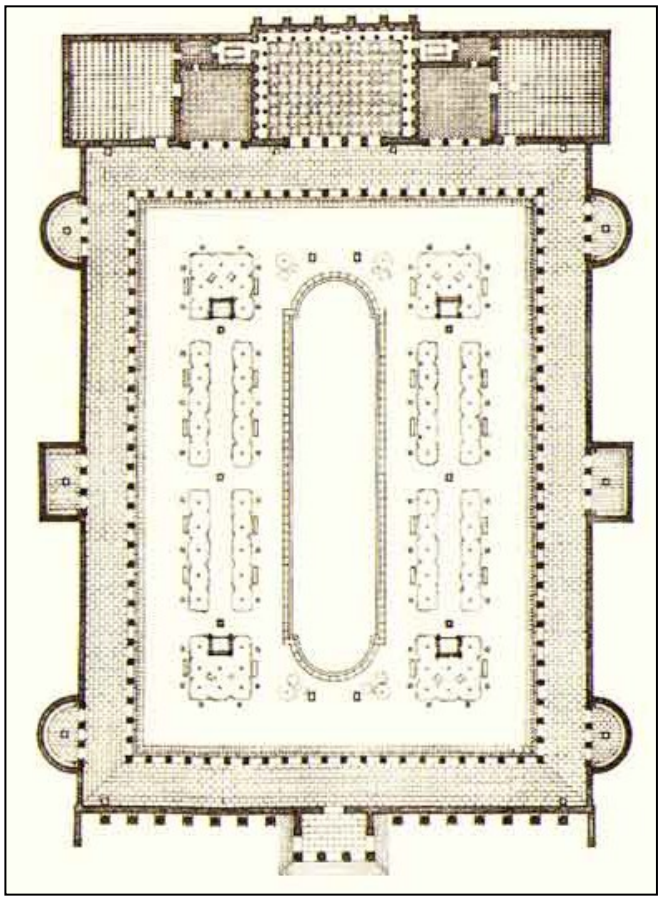

Fig. 2: Plan of the original building of the Library of Hadrian (people.duke.edu, 2016).

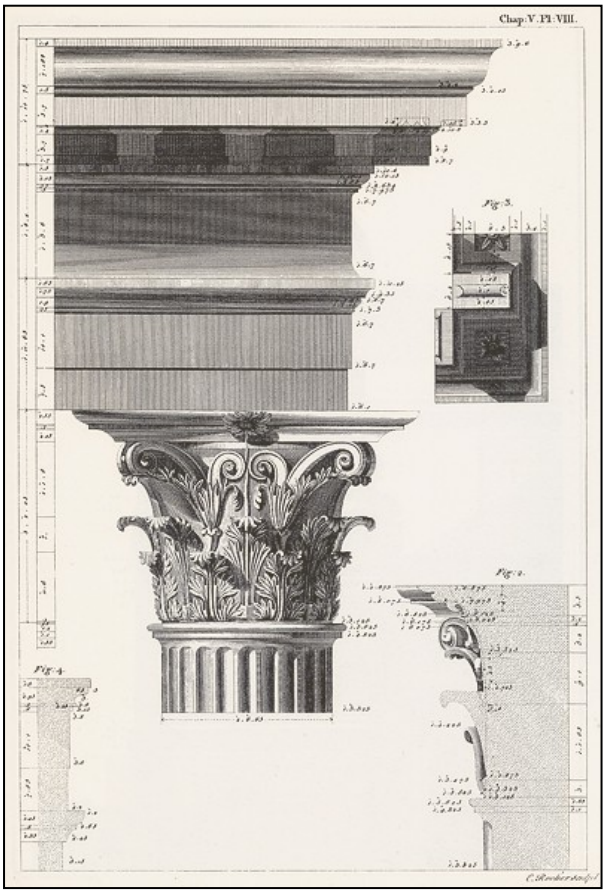

Fig. 3: Drawing of a Corinthian plate of the western façade (Stewart & Revett, 2007).

2.b Building materials of the monument

The Library of Hadrian was constructed of multiple materials, differentiated according to the purpose of their use. The external side of the Library was almost entirely built in cheap Poros blocks, a hard, thin-bedded and cream-colored limestone (United Nations, 2003). The only exception was the western façade, where the main entrance of the building was located. As described by Pausanias, who visited the area, the Propylon was decorated with four columns of Phrygian marble, creating a porch in front of the main entrance. The wall of the western façade was built entirely in Pentelic marble, while the fourteen Corinthian columns decorating the façade were made of Karystos stone (Pausanias, 1918; Sourlas, 2011).

The remaining area, still visible today, is the northern part of the western façade, immediately adjacent to the main entrance of the building. It consists of the remaining wall built in Pentelic marble and seven Corinthian columns constructed of green Karystos marble (Fig. 4). A brief description of the basic properties of these stones follows, as these are the materials under investigation in this study and their chemical composition plays a major role in the interactions with the atmospheric pollutants.

2.b.1 Pentelic marble

Marble, in general, is a metamorphic rock, composed of recrystallized carbonate minerals, under great heat and pressure. It is a compact and close-grained type of limestone, superior in quality from other calcareous substances. The term *Pentelic* derives from the quarries in Mount Pentelikon, situated northeast of Athens, being the primary source of white marble since the late 6^{th} century BC. It was used for decorative or construction purposes and it was preferred by artists due to its beautiful, clear white color. Later on, it was exported throughout the Roman Empire or used by the ruling Romans in the Greek area, as is the case in Hadrian's Library (Fig. 4) (Jameson, 1816; Bingley, 1821; Dinsmoor, 1950; Blatt & Tracy, 1995; Fant, 1995).

Pentelic marble has a relatively coarse grain size and shows intense crystallization, with thin laminae parallel to the slight schistosity of the rock. Calcite ($CaCO_3$) is its primary mineral constituent, with accessory muscovite and traces of quartz. As shown in several studies, it is primarily composed of calcite (96-98.5%), with minor impurities, such as Al, Si and Fe oxides, attributed to muscovite [$KAl_2(AlSi_3O_{10})(F,OH)_2$], quartz ($SiO_2$) and hematite ($Fe_2O_3$) mineral formations, respectively (Dermentzopoulos, et al., 1988; Moropoulou, et al., 1998; Garrison, 2003; Maravelaki-Kalaitzaki, 2005).

2.b.2 Karystos marble

Karystos marble, also known as Cipollino marble, is a variety of marble quarried in several locations on the southwest coast of the island of Euboea in Greece. It has characteristic green wavy ribs on a white-green base. It was first used in ancient Greece and then imported to Rome from the 1st century BC onwards, mainly for decorative purposes, in the construction of columns, column shafts, plates and sculptures (Mastrapas, 1999).

The mean chemical composition of Karystos blocks, as presented by Laskaridis and Patronis (2009), shows an expected prevalence of Ca (47%), followed by Si (7.4%), aluminum (1.75%) and Fe (1.15%) and other trace elements, such as Mg, Mn, K, Na and Ti[1]. Its mean calcitic grain size is 0.2 mm. The mineralogical composition of Karystos marble, according to the same authors, shows a lower percentage of calcite (83-93%), compared to Pentelic marble. It also shows a high content of muscovite (2-5.5%) and chlorite (ClO_2) (1.5-5.5%), minerals that contribute to the characteristic green color of this material. Other minerals present are albite ($NaAlSi_3O_8$) (1-4%) and quartz (1-6%).

Fig. 4: Western façade with areas built in Pentelic marble (A) and Karystos marble (B) (Personal archive).

[1] Note that another 40% of the mentioned mean chemical composition was loss in ignition (L.O.I.), due to the analytical procedure.

2.c Effects of air pollution on marble

Decay of monuments in urban sites showed a significant acceleration during the last decades. This change has been attributed mostly to the sharp increase of air pollutants. Such substances, when added to the environment at a rate faster than they can be dispersed, diluted, decomposed, recycled, or stored in a harmless form, are termed as pollutants. As a result, air pollutants can be described as substances that cause a change in the normally expected composition of air. They do not occur naturally in the atmosphere and if so, they are in quantities exceeding those of the standard composition. Therefore, they can include almost any natural or artificial matter capable of being airborne; solid particles, liquid droplets, gases or mixtures of these forms (Amoroso & Fassina, 1983; Nathanson, 2015).

Air pollutants are classified into primary and secondary pollutants, according to the process involved in their creation. Primary pollutants are directly emitted into the atmosphere by the pollution sources. Secondary pollutants are substances that derive from primary pollutants, after their physicochemical alteration in the atmosphere. According to their physical form, atmospheric pollutants are divided into particulate matter (PM) (dusts, fumes and smokes), gaseous pollutants (gases and vapors) and odors (Kjellstrom, et al., 2006; EMEKA, 2011).

This study is focused on gaseous pollutants and particulate matter and its fractions ($PM_{2.5}$ and PM_{10}), as they have a severe effect on the decay rate of materials. Description of the decay mechanisms and the role of each pollutant type in the formation of black crust is fundamental in recognising the level of their participation (Brimblecombe, 2016).

2.c.1 Gaseous pollutants

Pollutants of this category are present in the atmosphere in the form of gas molecules. There are several gaseous pollutants that take part in the deterioration process of monuments, such as sulfur dioxide (SO_2), nitrogen oxides (NO_x) and ozone (O_3). When considering the black crust formation, each pollutant plays a different role, with differentiations in both the time and the form in which they affect the material. This process involves multiple interactions between the pollutants, the atmosphere and the material. It is usually characterized by a great variability in the final effect, also depending on other factors, such as temperature, precipitation and solar radiation of the area and the pH levels of the interaction surfaces (Amoroso & Fassina, 1983; Rodriguez-Navarro & Sebastian, 1996; Ozga, et al., 2011).

Gaseous sulfur has either natural or anthropogenic sources. Sulfur dioxide in particular, is the most important gaseous atmospheric constituent setting the formation of black crust in motion. It is a chemical compound that is released into the atmosphere through combustion of fuels (EMEKA, 2011). Such combustion processes may be due to gasoline or diesel engines, coal-fired power plants and refining of crude oil (Gaffney & Marley, 2009). When it has reached the atmosphere, SO_2 is oxidized into sulfur trioxide (SO_3) through the following reaction:

$$2SO_2 + O_2 \rightarrow 2SO_3 \qquad (1)$$

As SO_3 is highly soluble in water, it forms droplets of sulfuric acid (H_2SO_4), when the amounts of water vapor are sufficient. The following hydrolysis reaction occurs:

$$SO_3 + H_2O \rightarrow H_2SO_4 \qquad (2)$$

In the presence of humidity, sulfuric acid reaches the marble surface in areas protected from rain, through condensation. There, it attacks the material (calcite in particular) and forms gypsum with a simultaneous release of carbon dioxide (CO_2), by means of the following reaction:

$$H_2SO_4 + CaCO_3 + H_2O \rightarrow CaSO_4 \cdot H_2O + CO_2 \qquad (3)$$

As a result, gypsum nucleation points are produced. This form of weathering leads to the formation of the so-called *black crust*. When the crust has reached a considerable depth, it can detach from the marble surface and create a new, unaltered and unprotected surface. Subsequent formation of new crystals after the loss of the initial crust leads to the formation of a new crust, in an ever-repeating process (Camuffo, et al., 1982; Rodriguez-Navarro & Sebastian, 1996; Steiger, 2003; Fronteau, et al., 2010).

The process described above can be greatly -although indirectly- affected by the presence of other gaseous pollutants, such as nitrogen oxides and ozone. Nitrogen oxides are created through dissolution of nitrogen and its reaction with oxygen during combustion processes, with the main source being diesel engines (Gaffney & Marley, 2009). Naturally, they are very stable compounds and enter chemical reactions only under high temperature and pressure. Nitrogen dioxide (NO_2) has a catalytic role in the oxidation of SO_2 on the marble surface (Johansson, et al., 1988), which can occur through the following reaction:

$$NO_2 + SO_2 \rightarrow NO + SO_3 \qquad (4)$$

Therefore, a shift in NO_x emissions can lead to a change in the oxidation rates of SO_2, affecting black crust formation and growth in an indirect manner. Gypsum formation can also occur through nitrification of carbonate minerals, but not in a considerable level. Additionally, black crusts are typically created in areas of monuments that are protected from rainwater washing, therefore aiding the action of highly soluble nitrogen compounds (Amoroso & Fassina, 1983; Sanjurjo-Sánchez & Alves, 2011).

Ozone (O_3) is also greatly affected by NO_x concentrations, as its destruction in the stratosphere is catalyzed by NO and NO_2. This has, in turn, an effect on SO_2 oxidation capacity. According to Penkett et al. (1979), the rate of sulfate formation from SO_2 and O_3 is 1000 times faster than with SO_2 and oxygen, thus setting another indirect effect on the black crust formation (Charola & Ware, 2002).

2.c.2 Particulate matter

Although the formation of black crust, as described in the previous subchapter, primarily involves SO_2 and is regulated by NO_x and O_3 concentrations, it is particulate matter (PM) that plays a very important role in facilitating the whole chemical process. Particulate matter involves any microscopic substances that can be airborne in the atmosphere. They can be produced either by disintegration of solid or liquid matter (e.g. dust or sea spray) or by condensation from the gas phase (e.g. smoke from industry) (Amoroso & Fassina, 1983). The main anthropogenic sources include burning of fossil fuels in vehicles and industrial processes and domestic heating (Fellenberg, 2000). In the field of stone decay studies, they are usually classified into two main categories, according to their size. Coarse PM with an aerodynamic diameter larger than 2.5 μm and less than 10 μm, is defined as PM_{10}, while fine PM with an aerodynamic diameter less than 2.5 μm, is defined as $PM_{2.5}$ (EMEKA, 2011; Omidvarborna, et al., 2015).

Depending on their origin, atmospheric particles may include elemental carbon and a series of adsorbed substances, such as heavy metals, organic compounds, silicates (Al_2O_3, SiO_2), salts (sulfates, nitrates), etc (Valavanidis, et al., 2006). These particles can reach the marble surface through dry deposition, as dust. As this dust can be rich in clay minerals and therefore have a high porosity, it can retain high levels of humidity, while at the same time it prevents quick evaporation of the water penetrating the surface of the porous calcitic substrate (Rodriguez-Navarro & Sebastian, 1996; Ozga, et al., 2013).

The sulfating process of SO_2, as described earlier, can be accelerated in the presence of carbonaceous particles and some transition and other metals, such as Fe, V, Cr, Ni, Pb, etc. These metals act as catalysts in the oxidation (1) and hydrolysis (2) reactions of SO_2. (Rodriguez-Navarro & Sebastian, 1996). After each sulfation cycle, the newly created gypsum aggregates fixate the atmospheric particles, ensuring the presence of catalytic transition metals and carbonaceous particles. The entrapment of the latter into the crust matrix is responsible for the unsightly coloration of the marble surface, as showed in multiple cases (Bonazza, et al., 2005; Maravelaki-Kalaitzaki, 2005; Sanjurjo-Sánchez & Alves, 2011; Prieto-Taboada, et al., 2013; Perez-Monserrat, et al., 2016).

2.d Air pollution and environmental conditions in Athens

Athens has always been a large social, economic and political centre in the Greek area, from ancient times until the present day. It has been continuously inhabited for at least 7,000 years, with a current urban population of about 3 million people. Its role as the capital of Greece was accompanied by the rapid increase of the city's population in the 1950s and '60s, during Greece's transition from an agricultural to an industrial nation. Athens is associated with intense polluting anthopogenic activities, as 50% of the national vehicle fleet and 40% of the industrial activity of Greece are confined in the Greater Athens Area (Kalabokas, et al., 1999; Tung, 2001; Hellenic Statistical Authority, 2011).

The Greater Athens Area (GAA) includes the cities of Athens and Piraeus and is located in a basin surrounded by mountains, except from its southwestern side, where it is open to the Saronic Gulf. As air pollution impacts are differentiated according to the climatic conditions of a region, it is important to mention that the complex topography of the area leads to local atmospheric circulations. During the 1982-1994 time period, the development of such circulations was found to be crucial in the accumulation of pollutants in this area, affecting their transport and dispersion and favoring air pollution episodes. High temperature and solar radiation (characteristic for the climate of this area) also play an important role, favoring intense photochemical processes and, therefore, secondary pollutant production (Assimakopoulos, et al., 1992; Kassomenos, et al., 1995; Bityukova, 2006; Vrekoussis, et al., 2013).

The main pollution sources in the GAA are automobile traffic, industrial regions close to the city of Athens and central heating. Traffic is considered as the main source of carbon monoxide (CO) and nitrogen oxides (NO_x). Industry is the main source of sulfur dioxide (SO_2) and suspended particles. The most important industrial units in the area are two refineries, one fertilizer plant, two iron steel plants and one cement plant. There are also about 100 medium-sized industries, related to food processing, plastic and textile production (Kalabokas, et al., 1999).

Changes in the pollutant emission and concentration in the atmosphere can be helpful in understanding the development in the decay of Cultural Heritage. Such changes were noticed in Greece, either because of changes in the industrial inventory (shut down factories, change in material processing) or changes in regulative measures decided by the European Union (EMEKA, 2011).

In particular, SO_2 emissions in Greece, mainly from fossil fuel combustion, showed a decrease of 9% during the 1990-2008 period. During the same period, emissions of CO decreased by 46%. Particulate matter emissions showed an increase of 22% in the $PM_{2.5}$ fraction and 31% in the PM_{10} fraction, during the 2000-2008 period (EMEKA, 2011).

Concerning the area in which the Library is located, data provided by the Ministry of Environment and Energy (2016) can attest to the diachronically favorable conditions for the growth of decay patterns in Cultural Heritage. In the latest annual report on atmospheric pollution, the Ministry provides data from the Athinas station –which is defined as urban-traffic-, concerning major pollutants from 1988 until 2015. Athinas street is located very close to the Library of Hadrian, adjacent to the Monastiraki Square, thus providing an ideal locale for the description of the surrounding conditions. Additional data for PM_{10} concentrations is provided from the Aristotelous station, which is also located in the centre of Athens and defined as urban-traffic, with similar conditions.

Regarding the Athinas station, the mean annual concentration values for SO_2 show a huge decrease of 88.1 % for the 1988-2015 period (Fig. 5). Concentrations were very high until 1992, with a rapid decline until 1995 and rather small variations until 2015. NO_2 mean annual concentration values show a decrease of 53.9 % for the 1988-2015 period, although still considered high until today. O_3 values show a decrease of 38.6 % during the 1990-2015 period. Finally, regarding the Aristotelous station, PM_{10} mean annual concentration values show a decrease of 25.5 %.

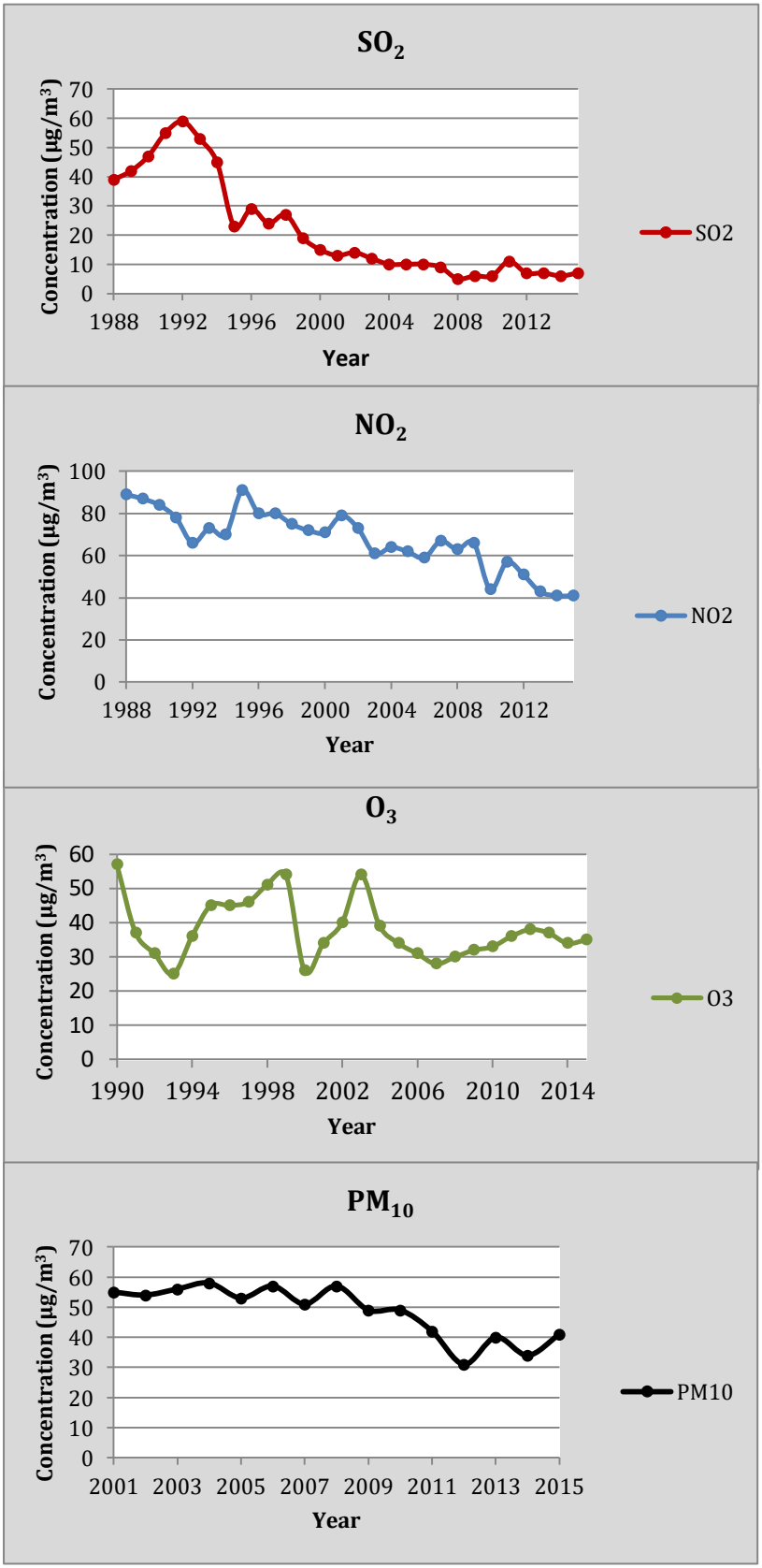

Fig. 5: Mean annual concentrations of SO_2, NO_2, O_3 and PM_{10} in the centre of Athens
(Ministry of Environment and Energy, 2016).

3. MATERIALS AND METHODS

3.a Sample collection and preparation

After permission was granted by the Ephorate of Antiquities of Athens, 5 samples of black crust were collected from weathered surfaces of the Library of Hadrian. The sampling area was at the northernmost corner of the western façade of the monument. Black crust areas were visible in the upper zone of the monument. Thick encrustations were accessible through a scaffold for conservation works (Fig. 6). This provided the opportunity to obtain samples from as high a level as possible. In urban settings, particulate emissions form traffic close to monuments are found in areas closer to the ground, whereas particles from distant sources are found in the upper areas (Janhäll, et al., 2009), meaning that the results regarding the source of the pollutants may be affected by the sampling location.

In total, five samples were collected, by detaching small fragments of black crust with the co-presence of stone substrate. The damage areas were scraped away using a scalpel, avoiding the removal of undamaged material as far as possible. Although the sampling area available was limited, an effort was made to have a variety in the geometrical setting, type of substrate and location of the samples, in order to possibly obtain comparable data.

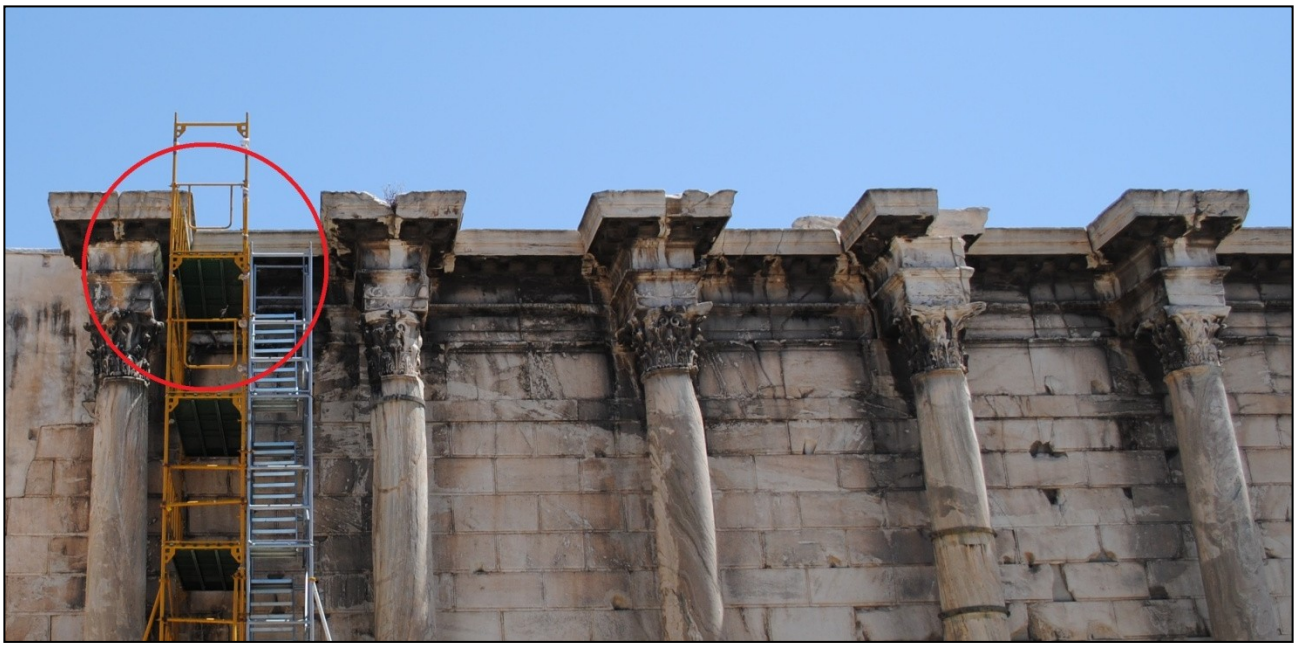

Fig. 6: Western façade of the Library of Hadrian with visible black crust areas in the upper level; sampling area noted in red circle (Personal archive).

All samples were taken from the area around the northernmost column of the western façade. Sample 1 (B1) was retrieved from the lower part of the architrave above the column. Sample 2 (B2) was taken from the southern part of the same architrave, on a vertical surface. Sample 3 (B3) was located on the upper level of the southeastern side of the column capital. Sample 4 (B4) comes from the body of the column itself. Finally, Sample 5 (B5) was obtained from the decorative ripple under the architrave stones, on the southern side of the column. Exact location of each sampling spot is shown in Appendix I-1.1 (See Appendices).

After the samples collection, preparation was needed, according to the analytical method. Small fragments of about 4 mm^2 in size were cut from samples B1 and B4, in order to examine vertical cross sections. This provided the opportunity to see possible alterations of the chemical composition or trace element concentrations in relation to the depth of the crust on the substrate. The fragments were embedded in Struers CaldoFix-2 resin, then dried at 75 ^oC for 1 hour and 30 minutes and polished using a Labopol-2 Polishing Device and multiple Struers grinding papers. The sections were then coated with a thin carbon tape in order to avoid electron overcharging.

Additionally, after the completion of all the analytical techniques and prior to the μ-XRF analysis, sample B1 was grounded to powder. The crust was scraped away from the substrate material using a scalpel and two different powders were pressed into tablets. The choice of this specific sample was based solely on its width and total weight and volume, permitting such a preparation. Finally, it should be noted that all samples - including the remaining fragments of B1 and B4 - were studied without any preparation for the rest of the analytical techniques.

3.b Analytical procedure

The analytical methodologies were planned according to the type of information that was needed. As explained in the previous chapter, black crust is a complex degradation product, with a large variability in the elements and processes involved in its formation. As a result, it is a demanding task to devise a set of methodologies in order to get complementary results. The main points of interest are the macroscopic and microscopic features (e.g. color, surface topology, size and shape of crystals etc.), elemental and molecular composition and differentiations of trace element concentrations in the samples. The ultimate goal is to link environmental pollution with the degradation products in Cultural Heritage and examine if they can be historic markers of past or present large scope changes in the atmosphere.

3.b.1 Optical Microscopy

All samples were examined under a LED I-Scope by Moritex in 10×, 50×, 200× magnifications, in order to have an initial approach on the fabric, color and morphology of the crust. Magnification of 50× also provided a polarized light image. This method was performed in the Laboratory of Archaeometry of the University of the Peloponnese, in Kalamata.

3.b.2 Micro Raman Spectroscopy

Micro Raman Spectroscopy provided information about the mineral phases present within the crust and substrate. Analyses were performed in the National Hellenic research Foundation, in Athens, using a Renishaw inVia Reflex dispersive confocal Raman microscope, with a 785 nm line of a Diode laser. The database used for the interpretation of the results were the e-VISART and e-VISARCH Raman spectral databases (Castro, et al., 2005; Pérez-Alonso, et al., 2006). Additionally, it was possible to detect inhomogeneities through the live microscopic image and get the molecular composition of each spot. This technique was applied to the polished cross section of sample B1.

3.b.3 Scanning Electron Microscopy

Chemical analyses on the samples were performed in the Laboratory of Archaeometry of the University of the Peloponnese, with a JSM-6510LV JEOL SEM (Scanning Electron Microscope), coupled with an Energy Dispersive Spectrometer (EDS) by Oxford Instruments. Quantification of the results was done using the INCA software. The spectra were acquired with a live time of 120 seconds, accelerating voltage of 20 kV and working distance of 20mm.

Line scans were obtained vertically, in order to see the variance of major elements from the surface to the inner side of the samples. For the surface analyses, a total of three measurements were made on both the crust and substrate surface of each sample. Then, the mean concentration of each element was calculated. For the bulk analyses on the polished cross sections of samples B1 and B4, a total of five successive measurements (50×50 μm) were obtained on each selected area, parallel to the surface of the sample, adding to a total area of 50×250μm. Mean concentrations were then calculated. The methodology was based on the work of Maravelaki-Kalaitzaki (2005).

Additionally, SEM images provided valuable information on the shape and size of gypsum crystals, general view of the crust matrix and both images and chemical composition of particles embedded within the crust layer.

3.b.4 Micro X-ray Fluorescence

Micro XRF spectroscopy was performed in the Institute of Nuclear and Particle Physics of N.C.S.R.[2] Demokritos, in Agia Paraskevi, Athens. This method was complementary to the previous, as it provided the same qualitative data, with the ability to evaluate the variability in presence of trace elements within the crust. The methodology used here was based on the assumption that the concentrations of trace elements (especially transition and heavy metals) would show variations from the surface to the inner part of the sample. A total of 4 line scans were performed on cross sections of samples B1 and B4 (two line scans on each sample). The measurement conditions for each line scan are presented in subchapter *4.e* of the *Results* chapter. Additionally, quantitative data were obtained by powdering the crust of sample B1 and pressing the material into a tablet. The quantification of the results was achieved through the application of the Fundamental Parameters (FP) approach, with an estimated uncertainty of ±15%. Finally, by preparing four reference tablets of fixed concentrations of $CaSO_4$ and graphite (10%, 20%, 35% and 50% of $CaSO_4$), estimation of the amount of carbon present in the crust was possible, along with an empirical estimation of S, Ca and $CaSO_4$ content.

[2] **N**ational **C**enter for **S**cientific **R**esearch

4. RESULTS

4.a Macroscopic observations

Before any analytical technique was performed, samples were measured, photographed and catalogued. First observations, without any use of technical support, may help in an initial categorization of the samples, where possible. It is also useful to investigate the state of preservation of the area of sampling, as it might give insight into the different types of crusts created on the marble surfaces. The terms used for the description of the deterioration patterns are based on the relative illustrated glossary published by ICOMOS-ISCS[3] (2008).

Sample B1 was collected from the lower horizontal surface of the architrave, completely sheltered from direct rainfall or water run-off. The marble block on which the sample was located, clearly shows signs of contour scaling and a thick crust covering almost the entire surface. The crust is darker in color in areas far from exposed surfaces (Fig. 7). The sample was collected from the darker area, on the edge of a contour scaling piece of marble. As a result, the crust encircles a thin substrate, previously exposed after material loss. It appears as a typical dendritic black crust, firmly attached to the substrate, with anomalous relief, high friability and considerable thickness (Fig. 8).

Fig. 7: Deterioration patterns in sampling area of sample B1 (Ephorate of Antiquities of Athens).

Fig. 8: Contour scaling in context with black crust (Ephorate of Antiquities of Athens).

[3] **I**nternational **CO**uncil on **MO**numents and **S**ites - **I**nternational **S**cientific **C**ommittee for **S**tone

Sample B2 was collected from a vertical surface of the same architrave as B1. Here, the deterioration patterns were different, with the main being granular disintegration leading to crumbling, and scaling. It appears that a thin laminar black crust covers the unaffected areas, whereas a more recent crust covers the areas exposed after material loss (Fig. 9). Sample B2 was collected from the exposed areas, in order to examine the initial evolution stage of such a crust. It appears as a thin dendritic black crust, highly friable and firmly attached to the deteriorated substrate (Fig. 10).

Fig. 9: Deterioration patterns in sampling area of sample B2 (Ephorate of Antiquities of Athens).

Fig. 10: Thin dendritic black crust on exposed surface after material loss (Ephorate of Antiquities of Athens).

Sample B3 was collected from the column capital, immediately underneath the architrave. The sampling spot is protected by direct rainfall or water run-off, but the seasonal presence of percolating water is possible. The area around the sampling spot shows intense granular disintegration, after material loss from mechanical stress and the growth of black crust on the surface of the exposed substrate (Fig. 11). Sample B3 includes a thick, compact black crust, with almost no relief and absence of marble substrate, grown in a scale-like macromorphology (Fig.12).

Fig. 11: Deterioration patterns in sampling area of sample B3 (Ephorate of Antiquities of Athens).

Fig. 12: Thick compact black crust in sampling spot of sample B3 (Ephorate of Antiquities of Athens).

Sample B4 was collected from a vertical surface of the column underneath the architrave, just below sample B3. The different material used for the columns (Karystos marble) and mechanical stress lead to massive bursting, crumbling and delamination, followed by the growth of a thin black crust. Delamination follows the marble veins patterns (Fig. 13). Sample B4 includes a thin dendritic black crust, with anomalous relief, encircling and firmly attached to an exposed piece of substrate, in an exfoliated area (Fig. 14).

Fig. 13: Deterioration patterns in sampling area of sample B4 (Ephorate of Antiquities of Athens).

Fig. 14: Dendritic black crust growth on thin exfoliated pieces of substrate (Ephorate of Antiquities of Athens).

Finally, sample B5 was collected from a horizontal surface of a decorative ripple, next to the column and architrave mentioned above. The sampling area shows significant deterioration, including material loss from mechanical stress on the upper left corner of the marble block. A thin black crust grows across the surface of the ripple (Fig. 15). Sample B5 includes a thin dendritic black crust, with anomalous surface, firmly attached to and following the relief of the substrate, which seems rather intact (Fig. 16).

Fig. 15: Deterioration patterns in sampling area of sample B5 (Ephorate of Antiquities of Athens).

Fig. 16: Thin black crust across the relief of the decorative ripple (Ephorate of Antiquities of Athens).

4.b Optical Microscopy

All samples were examined under a LED optical microscope, in order to describe the macro- and microstructure of the crusts and the substrates. Results were confirming the macroscopic observations in most cases.

In sample B1, a thick dendritic black crust is present, with globular aspect and visible inclusions, such as orange ferrous grains, opaque fly ash particles and dust deposits as quartz crystals (Fig. 17). An underlying substrate is also visible, showing micro-crystalline gypsum and calcite, including sparse embedded opaque particles close to the crust-substrate interface (Fig. 18). Immediately adjacent to the substrate is the intermediate layer of the black crust. As the crust encircles a thin piece of substrate, after the detachment of the sample, this layer was preserved and showed a gradual change in color and texture of the crust towards the substrate. A detailed view on this layer showed the presence of micro-crystalline gypsum, orange ferrous grains, opaque particles and salt crystals (Fig. 19-20).

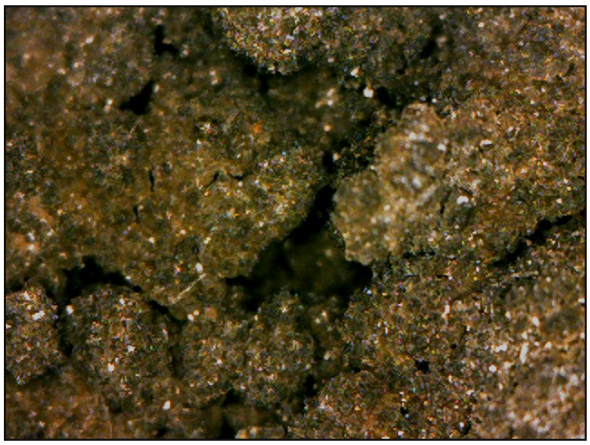

Fig. 17: Black crust on sample B1 (magnification 50×).

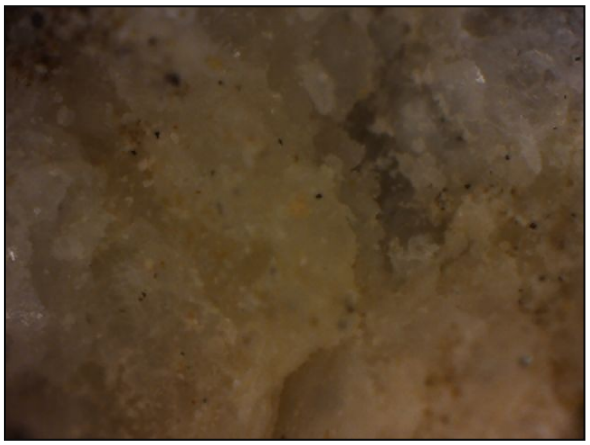

Fig. 18: Substrate of sample B1 (magnification 200×).

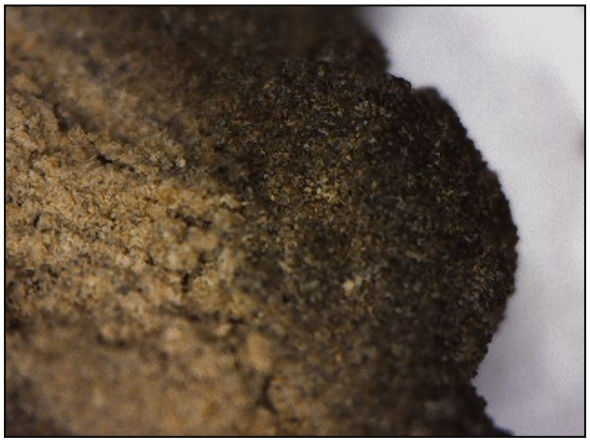

Fig. 19: Gradual change in color and texture of crust on sample B1 (magnification 50×, polarized light).

Fig. 20: Detail of intermediate layer in the black crust of sample B1 (magnification 200×).

Sample B1 also provided sufficient material to make a polished cross section. By examining the section under the optical microscope, information about the layers within the black crust and the interface between the crust and the substrate was available. The first observation was that the sample presented 3 distinct layers. The outermost layer is the dendritic black crust, highly inhomogeneous, with the gradual change in color shown from the examination of the loose fragment demonstrated in the cross section as well. A change in porosity and presence of aggregates and particles is present as well. The crust is more porous towards the substrate and more compact towards the surface. The orange ferrous grains and white quartz grains are more pronounced towards the substrate, whereas the opaque fly ash particles are increased towards the surface (Fig. 21). The crust strongly adheres to the substrate and there is a clear solution of continuity between the two layers. Immediately underneath the crust, the substrate shows a thin layer of microcrystalline gypsum, followed by almost unaltered marble (Fig. 22).

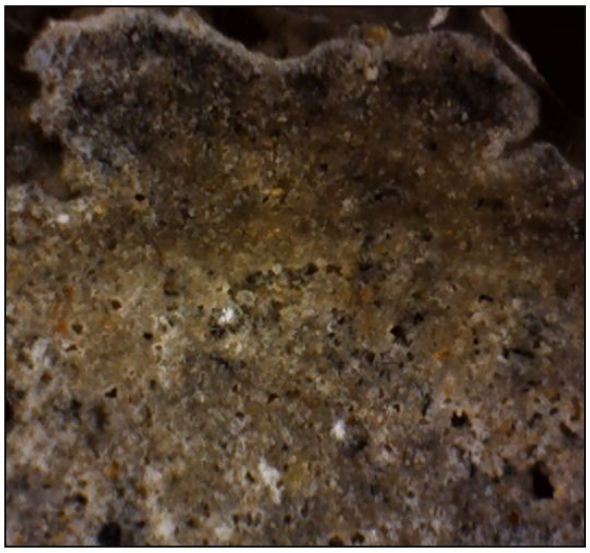

Fig. 21: Gradual change in color and texture within the black crust in sample B1 (magnification 200×).

Fig. 22: Interface between the black crust and the substrate in sample B1 (magnification 200×).

Due to the peculiar geometry of the sample, the crust encircling the substrate is visible underneath the marble substrate, with a much darker color. This layer resembles the outermost part of the dendritic black crust, so it is assumed that the crust growth was greatly affected by the conditions in a micro-scale. These include the geometry of the surface, the orientation of the growth of gypsum crystals and the cavity created by the contour scaling in the sampling spot.

Subsequently, the different capacity for humidity, exposure to air and light could encourage the growth of micro-organisms colonies or affect the growth pattern of a new crust over an exposed surface after detachment of older black crust etc. The examination of loose fragment showed a clear continuity between the dendritic black crust and the darker layer, which was found in small areas underneath the substrate. Additionally, the interface between the substrate and the darker shows a gradual change, as opposed to the sharp edge of the black crust (Fig. 24). This enhances the hypothesis that the innermost dark layer was either built up later than the external black crust, or that the conditions in a micro-scale did not favor the growth of a similar crust. In any case, the middle layer is considered as the substrate and the two adjacent layers are considered as different aspects of the same black crust (Fig. 23).

Fig. 23: Distinct layers in a cross section of sample B1 (magnification 50×).

Fig. 24: Interface between the substrate and the innermost dark layer in sample B1 (magnification 200×).

The crust present in sample B2 seems more recent, with globular formations on the surface and diversely colored areas; dark orange-brown areas inside the cavities and grey-black areas on the top of the globules. This possibly denotes an initial stage of black crust formation. Also evident is the presence of black fly ash particles, orange ferrous grains and white quartz grains (Fig. 25). The substrate seems slightly altered and includes macro-crystalline gypsum, calcite and quartz grains, along with black fly ash particles (Fig. 26).

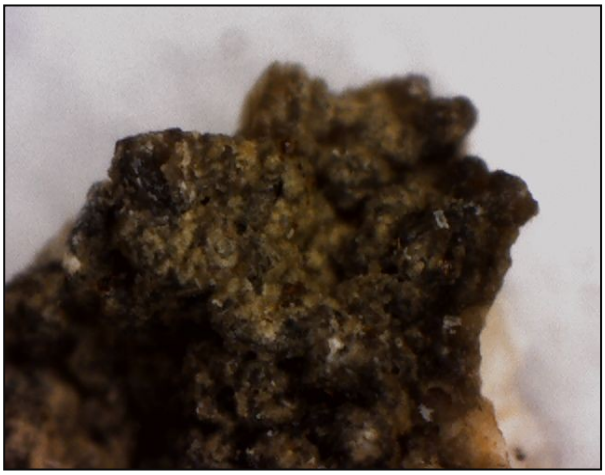

Fig. 25: Black crust on sample B2 (magnification 200×).

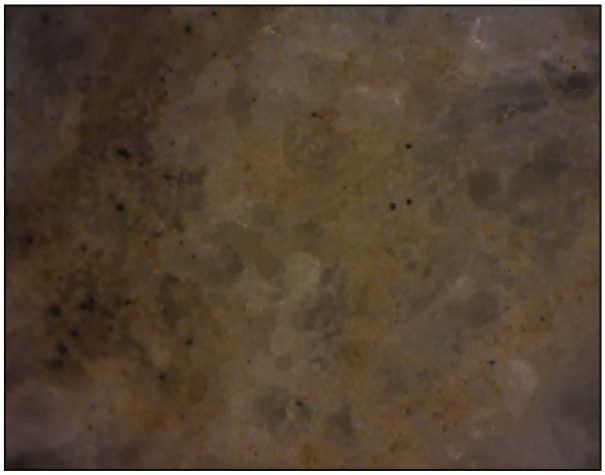

Fig. 26: Substrate of sample B2 (magnification 200×).

Sample B3 presents a thick, compact black crust, with almost no relief, compared to the others. Its color is dark brown in the lower levels, to black in the outermost areas. Orange (Fe) and white (quartz) particles are also present (Fig. 27). The substrate includes a deeper layer of the crust, with absence of marble material. A great number of grains and particles of various sizes and colors is present. They include salt crystals, orange ferrous grains, quartz grains, black fly ash particles and micro-crystalline gypsum and calcite (Fig. 28).

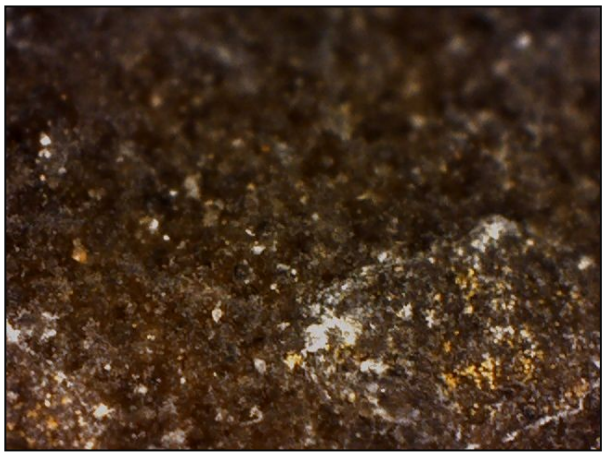

Fig. 27: Black crust on sample B3 (magnification 200×).

Fig. 28: Variety of grains and particles within the innermost layer of black crust on sample B3 (magnification 200×).

Sample B4 is a similar case with sample B1, in terms of growth of two different patterns of black crust on the same substrate. As mentioned earlier, the crust was formed in an already weathered piece of substrate, in the form of an exfoliated piece of Karystos marble. The external black crust is dark grey-black in color, with visible orange ferrous grains, opaque fly ash particles and quartz grains (Fig. 29). The substrate seems relatively sound, with large calcite crystals and rare inclusions present (Fig. 30). As in sample B1, the innermost dark layer adjacent to the substrate is a rather differently organized gypsum layer with the same aspect as the black crust. It gradually evolves to the dendritic black crust towards the edge leading to the external surface of the sample. Detailed view of this layer showed abundance of quartz crystals, opaque fly ash particles and ferrous grains as well (Fig. 31).

Fig. 29: Black crust on sample B4 (magnification 200×).

Fig. 30: Substrate of sample B4 (magnification 200×).

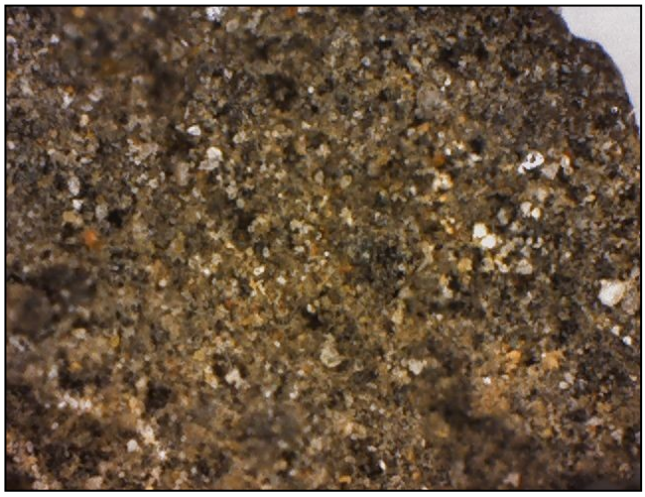

Fig. 31: Intermediate layer in sample B4 (magnification 200×).

As in sample B1, the material from sample B4 was sufficient to prepare a polished cross section. Here again, the exfoliated piece presents growth of dendritic black crust on both surfaces (exposed and covered surface). As a result, there are 3 identifiable layers, with the outer 2 layers being part of the same black crust, but with different growth patterns and in different evolution stages (Fig. 32). Detailed view of the interface between the substrate and the two external layers shows similarities with the case in sample B1. There is a gradual change in color and texture from the covered crust surface to the substrate, with no clear solution of continuity, whereas the exposed crust layer has a sharp edge with the substrate (Fig. 33-34). Further investigation on the matter is included in the following chapters, but it seems again here (as in B1) that the microclimate and conditions affect the growth of different patterns of black crusts, even on the same substrate and in a few millimeters distance from each other. Different chronological order of their growth should also be taken into consideration.

Fig. 32: Distinct layers in sample B4 (magnification 50×, polarized light).

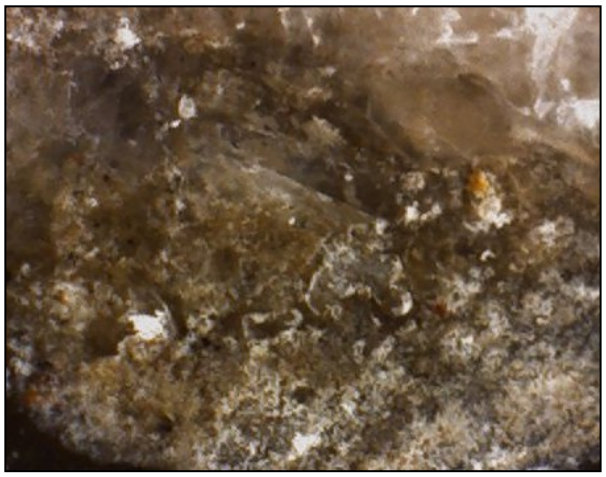

Fig. 33: Interface between the substrate and the innermost crust layer in sample B4 (magnification 200×).

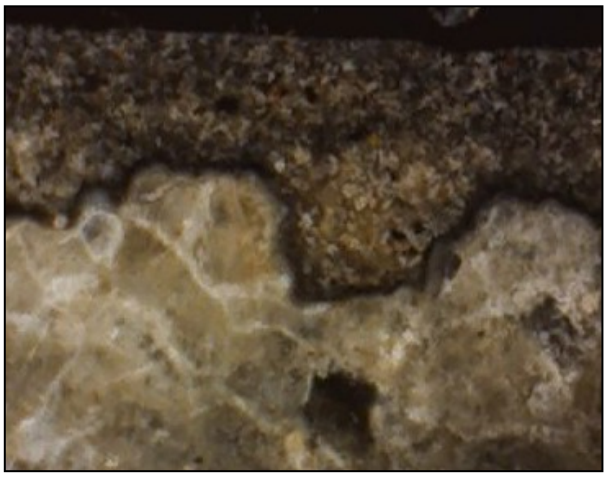

Fig. 34: Interface between the surface and the outer crust layer in sample B4 (magnification 200×).

In sample B5, there is a thin dendritic black crust visible. The crust follows the substrate relief and includes opaque fly ash particles, several quartz grains and some orange ferrous grains (Fig. 35). The substrate seems well preserved, with macro-crystalline calcite and some small gypsum crystals (Fig. 36).

After the macroscopic and microscopic examination of the samples, the results are summarized, along with a brief description in Table 1.

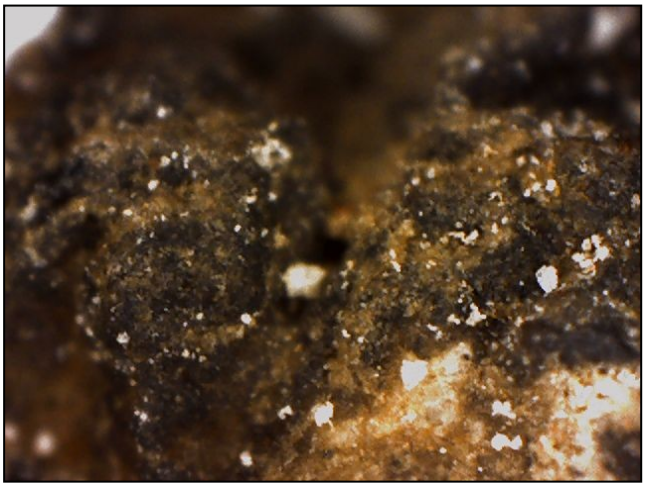

Fig. 35: Dendritic black crust on the surface of sample B5 (magnification 200×).

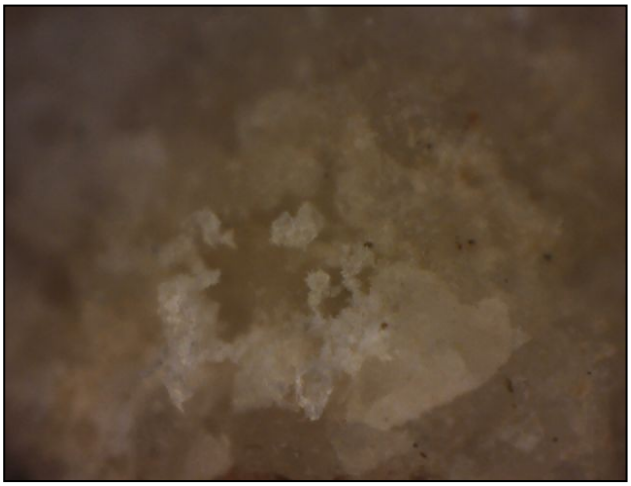

Fig. 36: Substrate of sample B5 (magnification 200×).

Table 1: Description and location of the samples

Sample	Location	Description	Substrate
B1	Western façade, lower horizontal surface of the architrave	Thick dendritic black crust and underlying substrate	Pentelic marble
B2	Western façade, vertical surface of the architrave	Thin globular dark brown crust and underlying substrate	Pentelic marble
B3	Western façade, curved surface of the column capital	Thick compact dark brown-black crust	Pentelic marble
B4	Western façade, vertical surface of the column	Thin dendritic grey-black crust and underlying substrate	Karystos marble
B5	Western façade, curved surface of a decorative ripple	Thin dendritic black crust and underlying substrate	Pentelic marble

4.c Micro Raman Spectroscopy

The polished cross section of sample B1 was examined under a μ-Raman microscope, in order to identify the main mineral phases and the molecular composition of inclusions in the gypsum matrix.

In sample B1, spot analysis on the interface between the external crust and the substrate confirmed that the boundary layer is mainly composed of gypsum (with characteristic Raman bands at 413, 495, 612 and 1008 cm^{-1}). The spectrum was obscured due to the crystalline nature of the analyzed surface and the presence of other impurities, rather than solely gypsum. Amorphous carbon (with its characteristic broad Raman band at 1300 cm^{-1}) and iron oxides (lepidocrocite γ-FeO(OH), with Raman bands at 212, 246, 304, 373 and 522 cm^{-1}) were also present (Fig. 37).

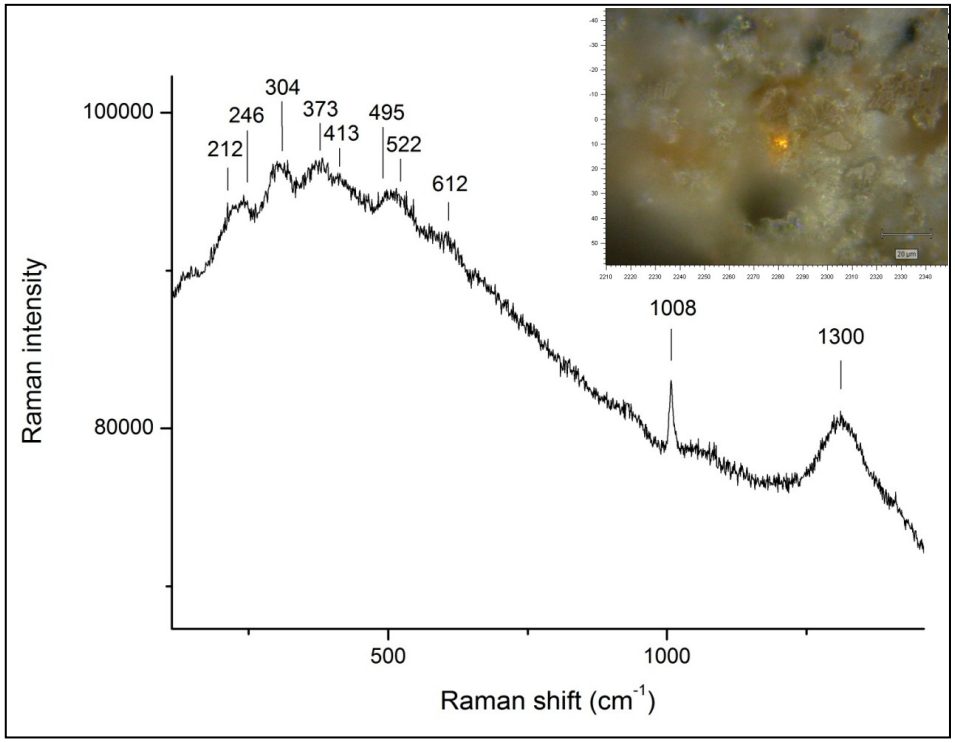

Fig. 37: Raman spectrum on the interface between the external crust and the substrate of sample B1: characteristic bands of gypsum, amorphous carbon and lepidocrocite (image of the analyzed spot on the top right corner).

In the interface between the substrate and both types of crusts, black particles were more pronounced, with an indicative spectrum showing they consist of vitrified carbon (sharp Raman bands at 1600 and 1300 cm^{-1}) (Fig. 38).

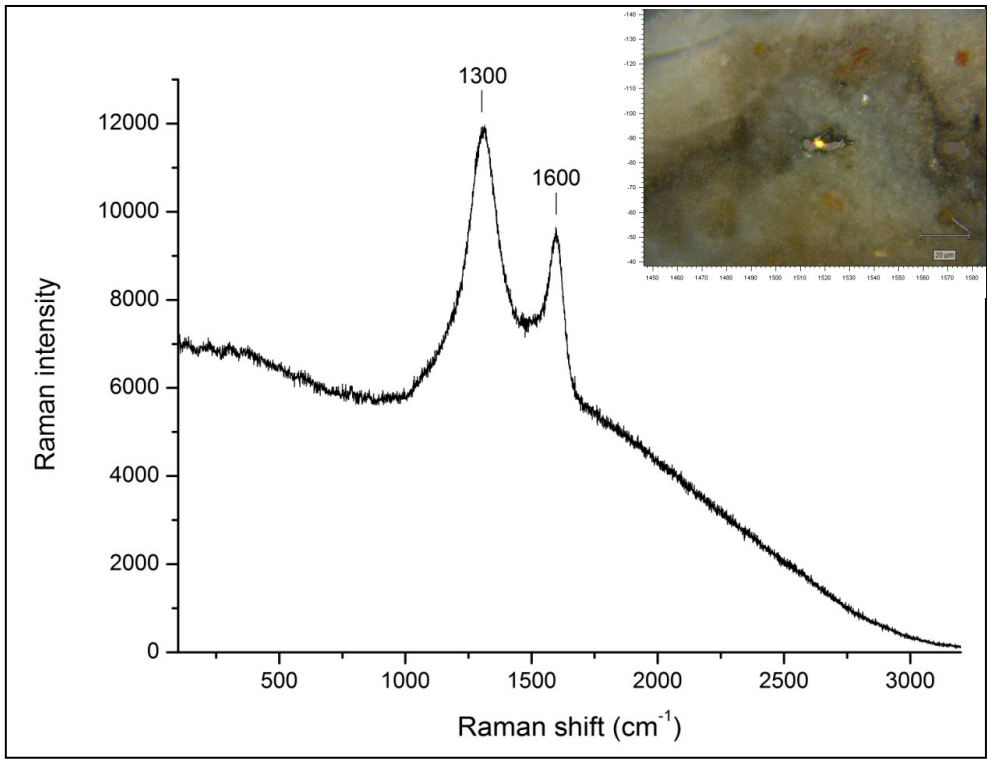

Fig. 38: Raman spectrum of black particles present in the gypsum matrix (image of the analyzed spot on the top right corner).

When examining the cross section under the microscope, both crusts in sample B1 showed a similar texture. Grains with the same color and texture and a diameter of about 20-30 μm were present in both layers. Several spot analyses on these grains showed that they are quartz crystals (characteristic sharp Raman band at 465 cm^{-1}), probably in contact with recrystallized calcite (characteristic Raman band at 1085 cm^{-1}) and other impurities, such as Fe oxides (lepidocrocite, weak Raman bands at 212, 246, 373, 522) (Fig. 39).

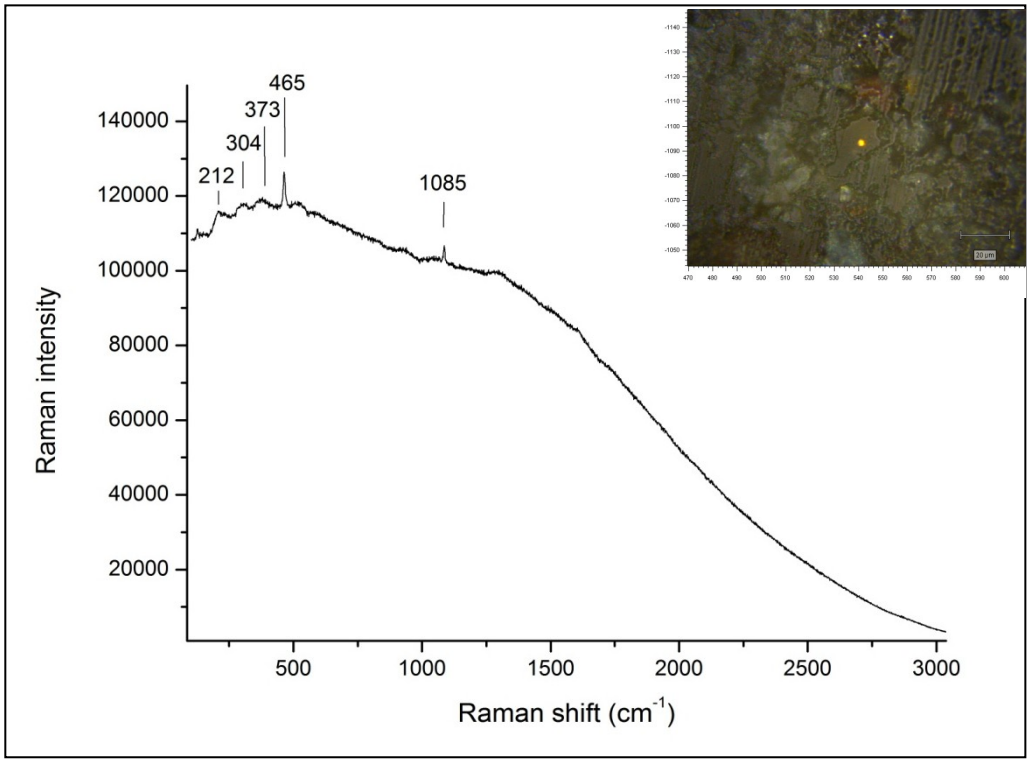

Fig. 39: Raman spectrum on the crust area, showing characteristics Raman bands for quartz, calcite and lepidocrocite (image of the analyzed spot on the top right corner).

Spot analysis in the middle of the substrate layer showed that it consists of pure calcite, with very clear and sharp bands at 281, 712 and 1085 cm^{-1}. Sharp bands at 154 cm^{-1} can be attributed to brookite (TiO_2), according to the literature (Morillas, et al., 2016) (Fig. 40).

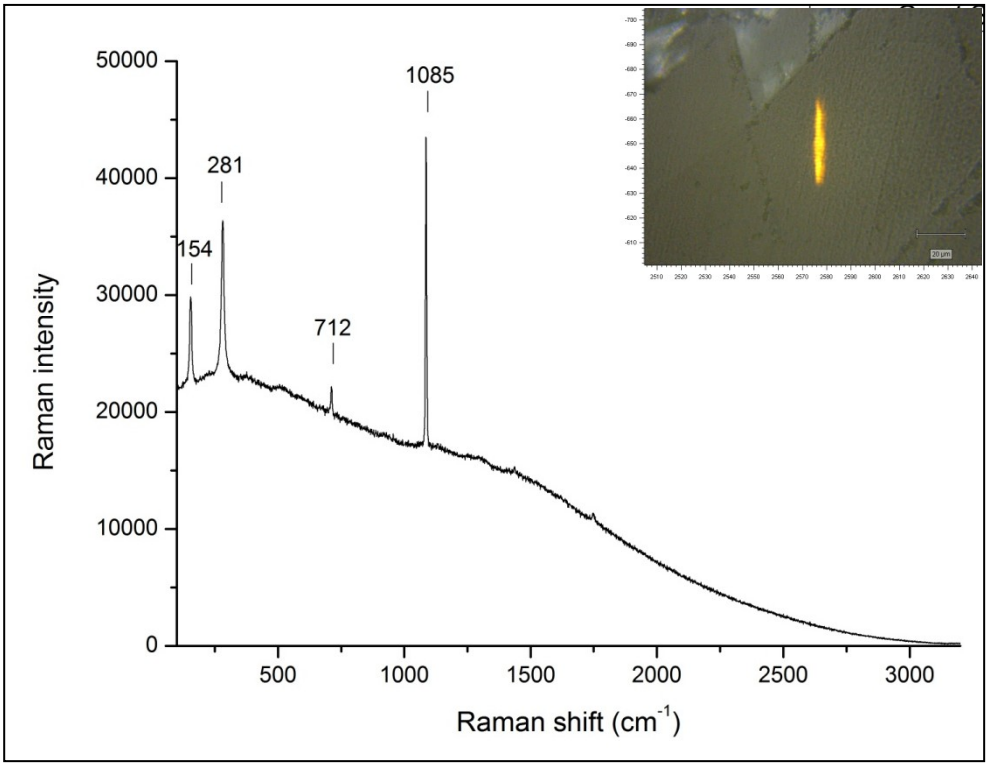

Fig. 40: Raman spectrum of the substrate, showing clear sharp bands of calcite and TiO_2 (image of the analyzed spot on the top right corner).

Finally, carbon was found in the two crust layers, both as individual particles about 15 μm in size and spread in the gypsum matrix, apparently as large number of smaller particles. Representative Raman spectra of the external black crust (Fig. 41) and its innermost counterpart (Fig. 42) confirmed their presence, along with other impurities, such as Fe oxides.

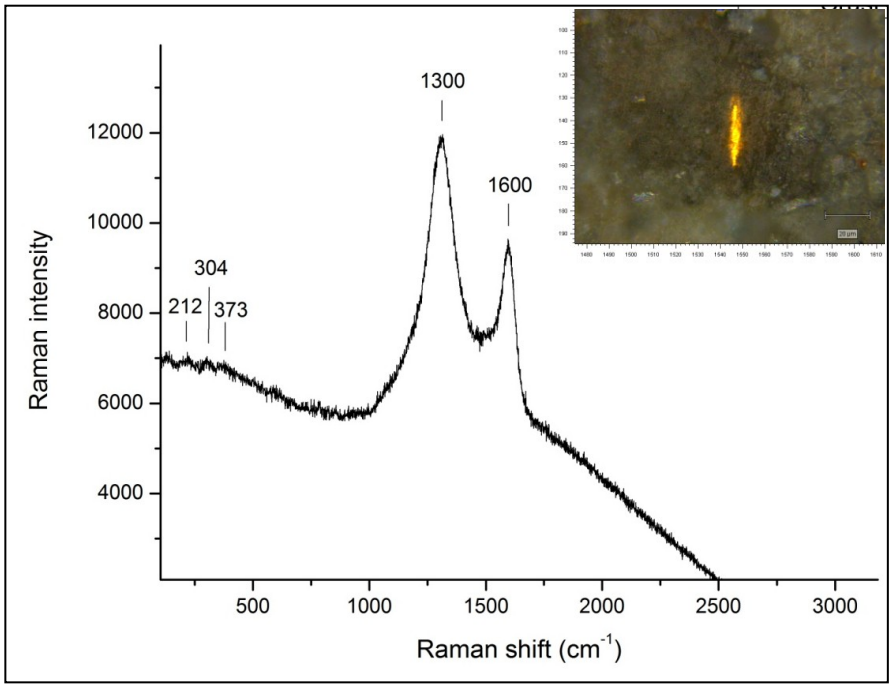

Fig. 41: Raman spectrum of the external black crust, showing characteristic sharp bands of carbon and weak bands of lepidocrocite (image of the analyzed spot on the top right corner).

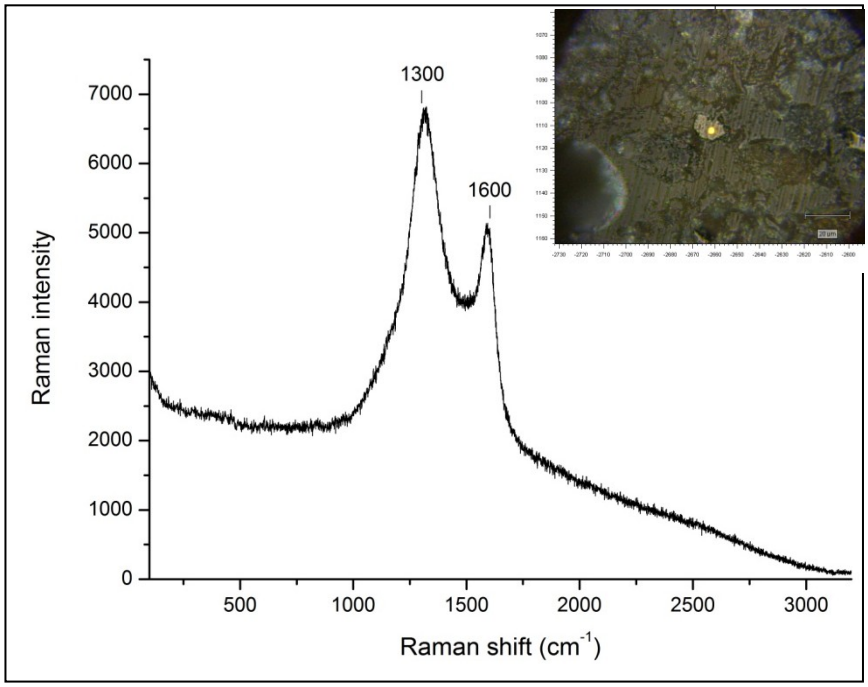

Fig. 42: Raman spectrum of the innermost crust layer, showing sharp bands of carbon on the spotted particle (image of the analyzed spot on the top right corner).

4.d Scanning Electron Microscopy

4.d.1 Surface and substrate chemical composition

As not all samples provided sufficient material for the preparation of polished cross sections, the chemical composition of the crusts and substrates was obtained from bulk analyses on the surface of the two layers of fragments of samples. It should be noted that the mean concentrations of oxides on the substrates referred to here may be either of altered substrate (marble and gypsum) or inside layers of the crusts, respectively to each sample. A summary of the results is presented in Table 2.

Table 2: Mean elemental composition of crust and substrate surfaces (in compounds %), obtained by SEM-EDS (C=crust, S=Substrate)

Sample	Na_2O	MgO	Al_2O_3	SiO_2	P_2O_5	SO_3	Cl	K_2O	CaO	FeO	Ba	PbO
B1-C	-	-	1.78	2.76	-	53.11	0.75	0.29	41.31	-	-	-
B1-S	6.04	-	-	4.59	4.16	41.6	5.4	1.14	37.06	-	-	-
B2-C	0.56	2.06	7.76	55.89	0.84	2.8	0.41	1.75	23.06	4.88	-	-
B2-S	-	2.1	3.73	12.15	-	10.92	-	-	71.1	-	-	-
B3-C	2.3	1.97	5.1	16.68	0.65	29.22	0.55	1.84	36.65	2.58	0.83	1.67
B3-S	2.26	1.93	5.71	21.47	-	25.41	1.8	1.72	36.67	3.34	-	-
B4-C	0.84	2.43	8.06	27.19	-	25.75	0.57	2	25.36	7.82	-	-
B4-S	-	1.77	3.56	9.43	-	8.11	1.31	1.59	72.31	1.93	-	-
B5-C	-	3.49	7.07	22.77	-	13.23	1.81	1.56	44.37	5.7	-	-
B5-S	-	-	-	1.9	-	18.33	-	-	79.77	-	-	-

The results show a similarity in the surface chemical composition of almost all crusts. For samples B1, B3 and B4, the major elements present are S and Ca, with the average values ranging from 25.75-53.11 % for SO_3 and 25.36-41.31 % for CaO. It is also evident that the range of values and the concentration ratio of these elements are rather constant.

The chemical composition of the black crust on samples B2 and B5 shows much lower concentrations of SO_3 (2.8 and 13.23 % respectively) and elevated values for SiO_2 (55.89 and 22.77 % respectively). All crust surfaces, except from sample B1, show significant values of FeO (ranging from 2.58-7.82 %), with the highest value detected in sample B4. K_2O and Al_2O_3 were present in all crusts, with values ranging from 0.29-2 % and 1.78-8.06 % respectively. Samples B2, B3 and B4 showed small amounts of Na and Cl. Finally, it should be noted that only in the crust of sample B3, Ba and PbO were detected (with values of 0.83 and 1.67 % respectively).

Regarding the substrates, the chemical composition confirmed the macroscopic and microscopic observations. A general increase in the values of Na and Cl is observed, along with the rather significantly pronounced presence of P_2O_5 in the substrate of sample B1 (4.16 %). An increase in the values of SiO_2 is accompanied by a decrease of SO_2 values and increase of CaO values. Specifically, samples B2, B4 and B5 showed CaO values higher than 70 % (71.1, 72.31 and 79.77 % respectively), indicating a different substrate, rather than a deeper layer of the crust.

4.d.2 Bulk chemical composition

Additionally to the surface analyses, polished cross sections of samples B1 and B4 provided the opportunity for bulk analyses on the different layers present within these samples, as mentioned in subchapter *3.b.3*. The mean elemental compositions of each area are presented in Table 3.

Table 3: Mean elemental composition of selected areas of samples B1 and B4 (in compounds %), obtained by SEM-EDS
(BC=black crust, S=substrate, IC=inner crust, BC1=outer layer, BC2=inner layer)

Sample	Na_2O	MgO	Al_2O_3	SiO_2	P_2O_5	SO_3	Cl	K_2O	CaO	TiO_2	FeO	CuO	ZnO	PbO
B1-BC1	0.67	1.29	3.48	15.76	0.53	43.36	0.26	0.86	31.57	-	0.97	0.12	-	1.13
B1-BC2	1.5	1.79	5.43	21.47	1.78	27.57	1.54	1.43	31.07	0.23	4.38	-	-	1.81
B1-S	1.22	2.17	0.47	0.47	1.15	3.53	0.24	0.13	89.59	-	-	0.16	0.4	0.51
B1-IC	3.07	3.77	8.82	27.48	7.84	8.38	4.15	2.94	28.13	0.55	2.77	-	0.21	1.9
B4-BC	1.09	2.44	5.11	18.32	2.1	29.09	0.39	0.94	36.56	0.19	1.99	-	0.12	1.65
B4-S	2	-	0.65	0.83	0.48	0.94	0.16	0.13	93.98	0.3	0.14	-	0.16	0.25
B4-IC	1.32	1.87	6.81	17.89	0.48	25.97	0.48	1.2	39.11	0.39	2.36	0.18	0.16	1.78

The main components of the external black crust of sample B1 are S, Ca and Si. There is a rather significant amount of metal oxides (such as Fe_2O_3 and PbO), salts (Na_2O and Cl) and aluminum. Other elements present in small amounts are Mg, K, P, Ti and Cu. There is a significant increase (15.79 %) in S content towards the surface of the crust and an increase of aluminosilicates, metal oxides, salts, Mg and P towards the substrate. Calcium levels are constant throughout the crust body, at about 31 %. The inner crust shows significant amounts of silica and aluminum compared to the black crust, along with elevated values for Na, Cl, Mg and K. Phosphorous shows significantly higher values (7.84 %) and sulfur shows very low values (8.38 %). Metal oxides are in similar amounts, as in the black crust. The substrate shows dominant values of CaO (89.59 %) and very small amounts of the other elements.

Sample B4 also shows S and Ca as the main components of the external black crust (29.09 and 36.56% respectively), followed by Si (18.32 %) and Al (5.11 %). Metal oxides are also present, such as Fe_2O_3 (1.99 %), PbO (1.65 %), and ZnO (0.12 %). The substrate is characterized by dominant values of CaO (93.98 %). The inner crust shows again SO_3 and CaO as the main components (25.97 and 39.11 % respectively), in similar amounts with the external black crust. Aluminosilicates, metal oxides and the other elements present are in similar amounts with the external crust, only with the exception of a notable decrease (1.62 %) in P content.

4.d.3 Micromorphology and particulate matter

In sample B1, the external black crust is characterized by well defined, lance-shaped or lamellar gypsum crystals (10-20μm), grown into rosettes and creating the macroscopic image of a typical dendritic black crust (Fig. 43).

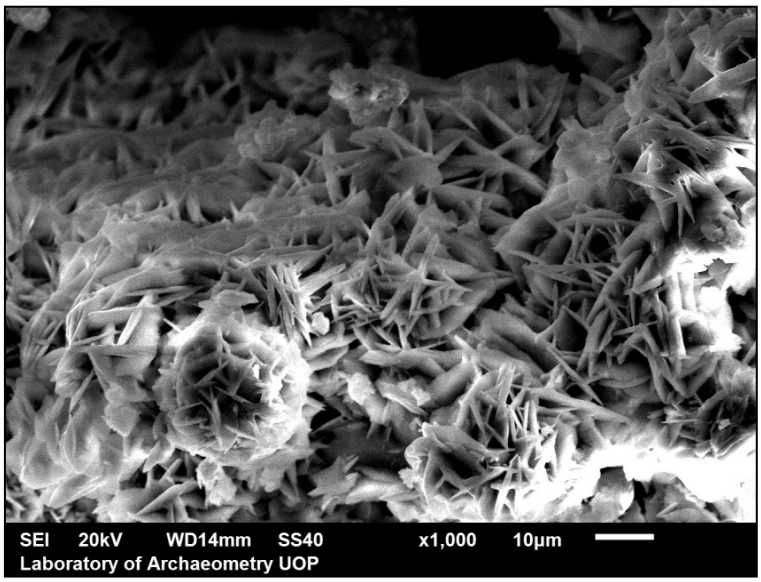

Fig. 43: SEM image of black crust surface on sample B1.

The particles detected on the crust surface of sample B1 include both smooth and compact Si-rich particles (~ 3 μm) and carbonaceous particles with a rough surface (~ 6 μm). According to the literature, the carbonaceous particles are accompanied by elevated S and Ca contents, even when carbon cannot be detected, and therefore are classified as such (Ozga, et al., 2011 and 2013; Perez-Monserrat, et al., 2016). It is interesting to mention that both particles are overgrown by gypsum and therefore act as gypsum crystallization nuclei, as observed from the relative SEM images (Fig.44).

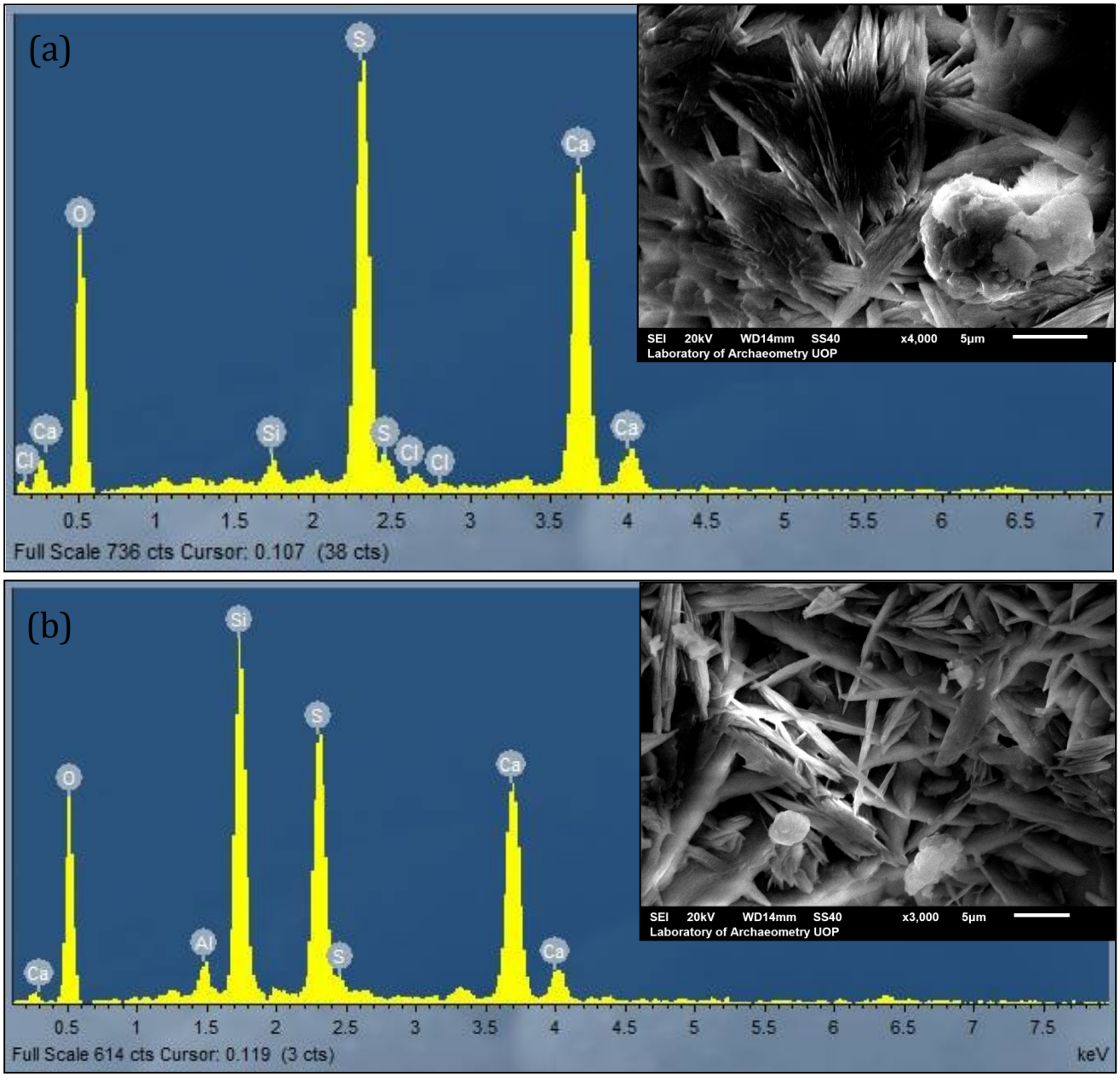

Fig. 44: Sample B1: SEM images and relative EDS spectra of (a) rough carbonaceous particles, rich in S and Ca, (b) smooth Al-Si particles.

It should be noted that during spot analyses in the polished cross section of sample B1, halite (NaCl) crystals were observed. The growth of these crystals appeared on both the substrate (Fig. 45) and the black crust (Fig. 46), all near the crust-substrate interface.

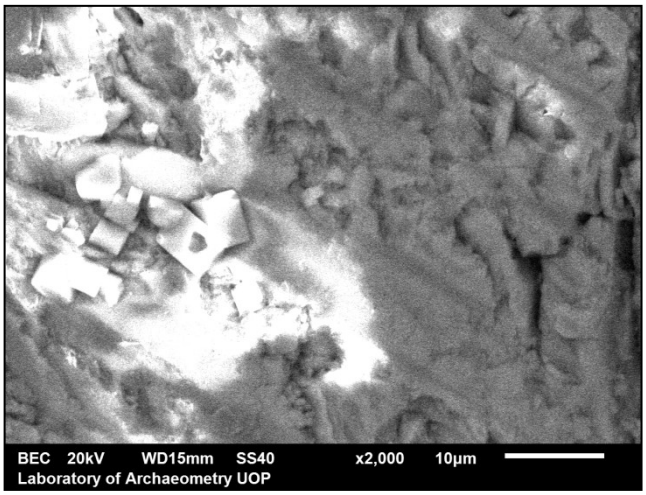

Fig. 45: Halite (NaCl) crystals observed in the substrate of sample B1.

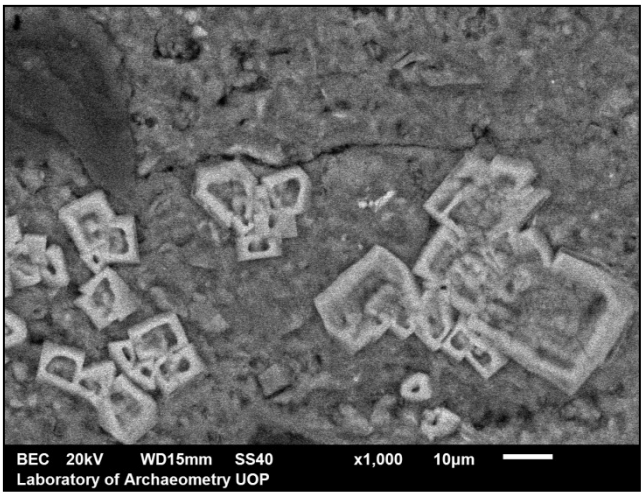

Fig. 46: Halite (NaCl) crystals observed in the crust of sample B1.

Additionally, in the same polished cross section and regarding sample B4, it was evident that the crust included reprecipitated calcite near the crust-substrate interface (Fig. 47) and quartz aggregates in the crust matrix (Fig. 48).

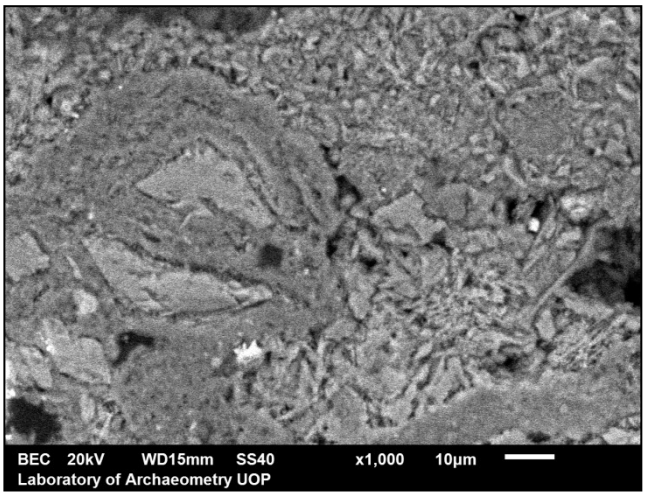

Fig. 47: Reprecipitated calcite observed near the crust-substrate interface in sample B4.

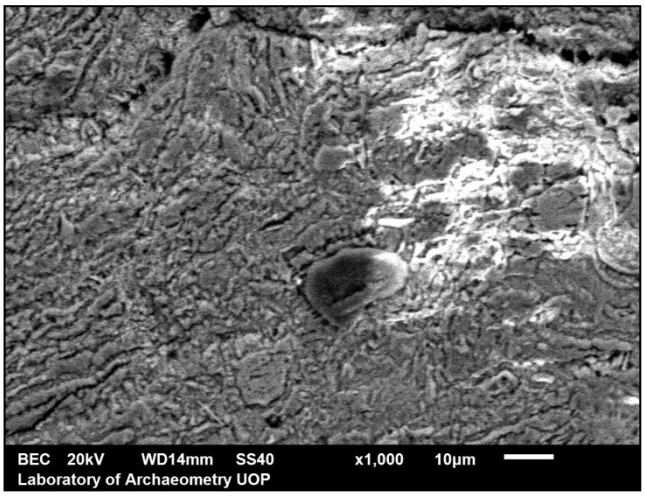

Fig. 48: Quartz aggregates observed in the crust of sample B4.

SEM images of the crust of sample B2 show a globular crust, with a flat top surface of the globules and a notable absence of macro-crystalline gypsum, probably grown in an already weathered marble substrate (Fig. 49). Ti-rich particles (~ 10 μm) were found near the surface of the crust, seemingly acting as gypsum nucleation points (Fig. 50).

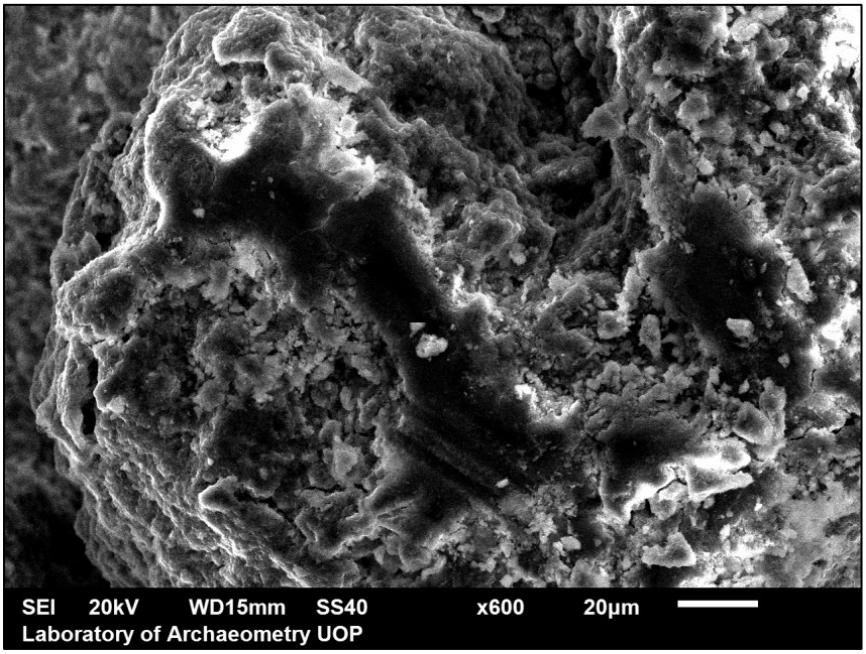

Fig. 49: SEM image of crust surface on sample B2.

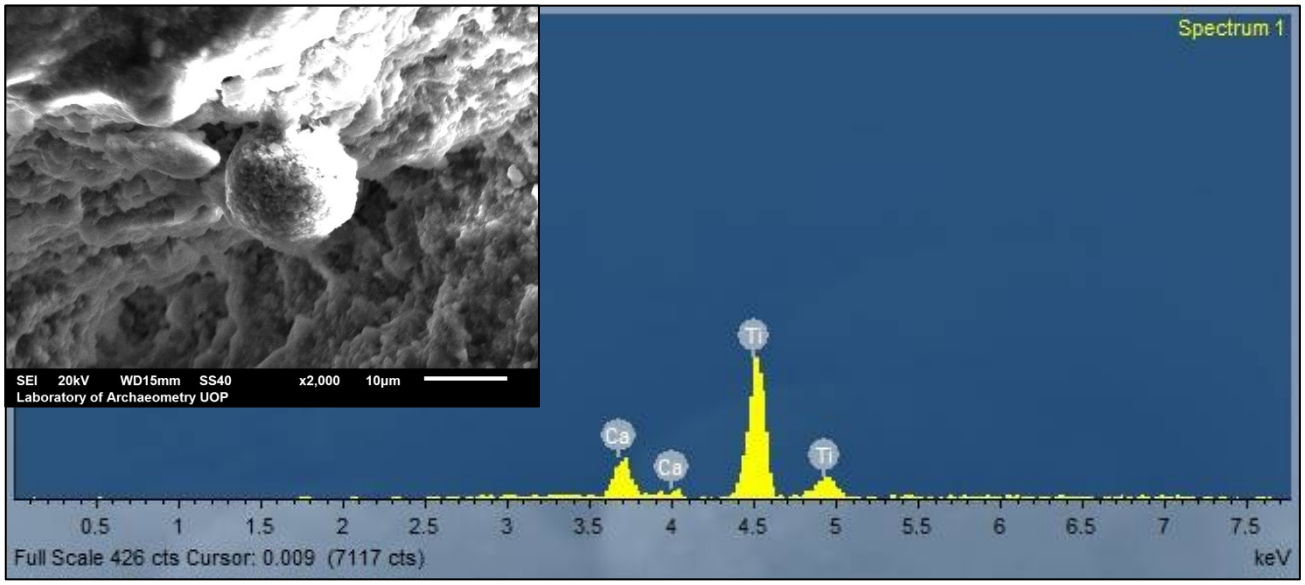

Fig. 50: SEM image and relative EDS spectrum of Ti-rich particle in the crust of sample B2.

Sample B3 shows a dense matrix of micro-crystalline gypsum (5-10 μm), with sparse elongated crystals (>10μm) and quartz grains (Fig. 51). The two types of particles identified here are porous carbonaceous particles (~ 5 μm) with high S and Ca contents and rough-dense carbonaceous particles (~ 10 μm), with high S and Ca contents (Fig. 52).

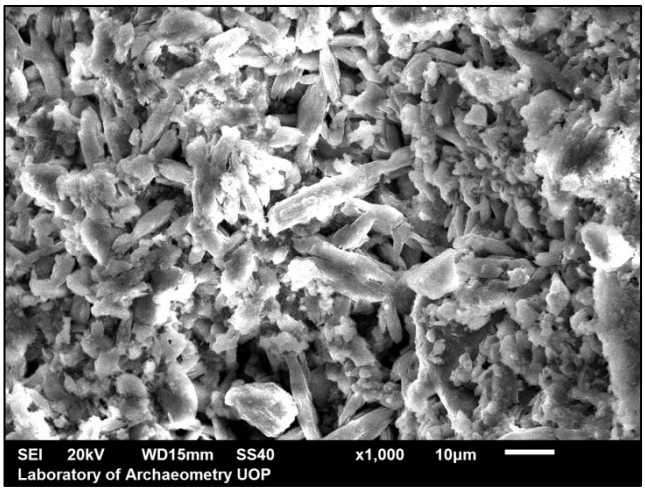

Fig. 51: SEM image of the black crust surface of sample B3.

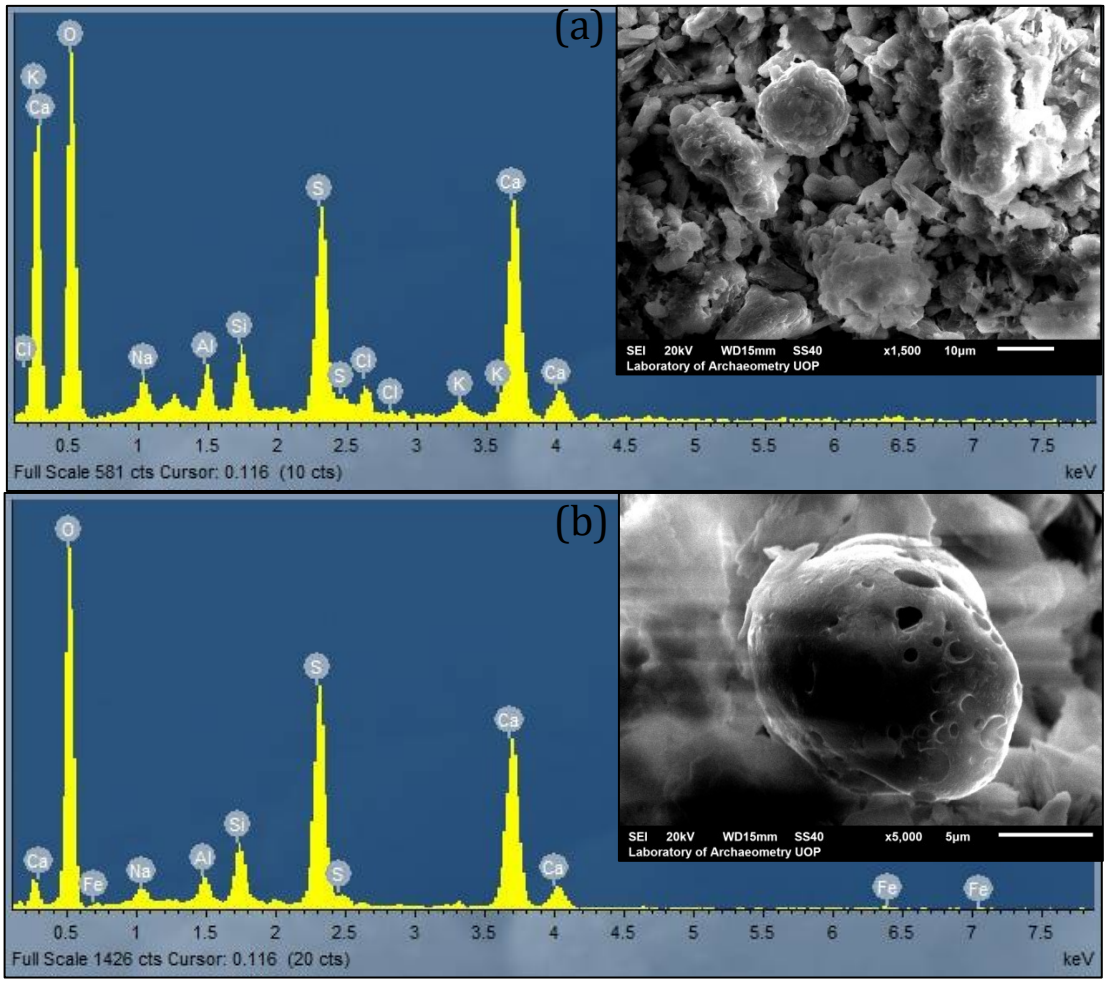

Fig. 52: SEM images and relative EDS spectra of (a) rough-dense carbonaceous and (b) porous carbonaceous particles, rich in S and Ca.

Sample B4 shows a rather dense gypsum matrix on the crust surface, mostly covered by depositions and with no visible macrocrystalline gypsum (Fig. 53). There are three typologies of particles identified in the crust: a) porous carbonaceous particles, rich in S and Ca (~ 10 μm) (Fig. 54), b) smooth and compact Si-rich particles (~ 3 μm), and c) smooth and compact titanium-rich particles (~ 6 μm) (Fig. 55).

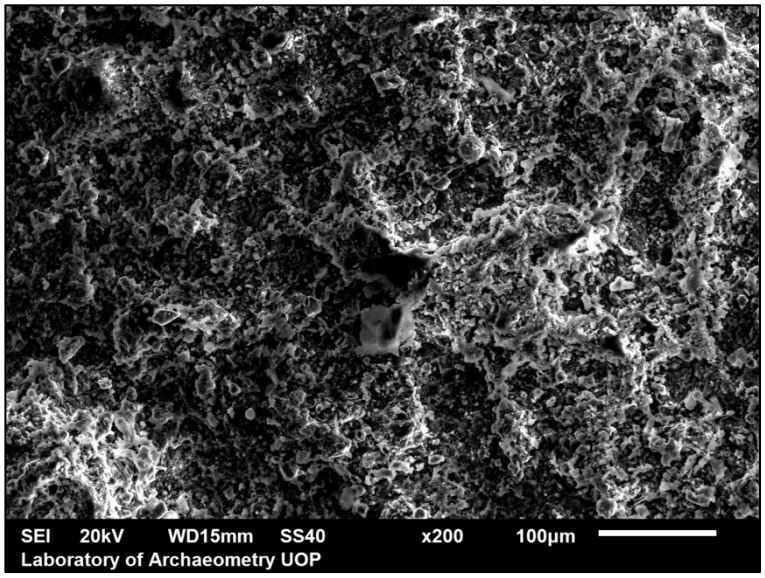

Fig. 53: SEM image of the crust surface of sample B4.

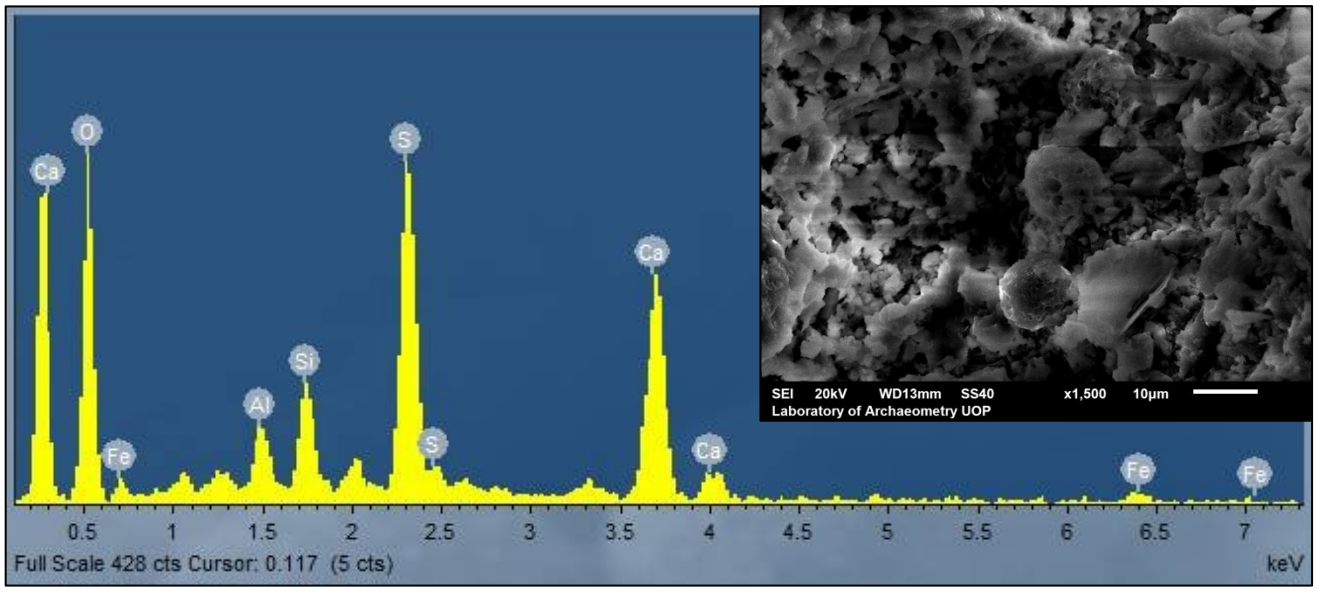

Fig. 54: SEM image and relative EDS spectrum of porous carbonaceous particles, rich in S and Ca, in sample B4.

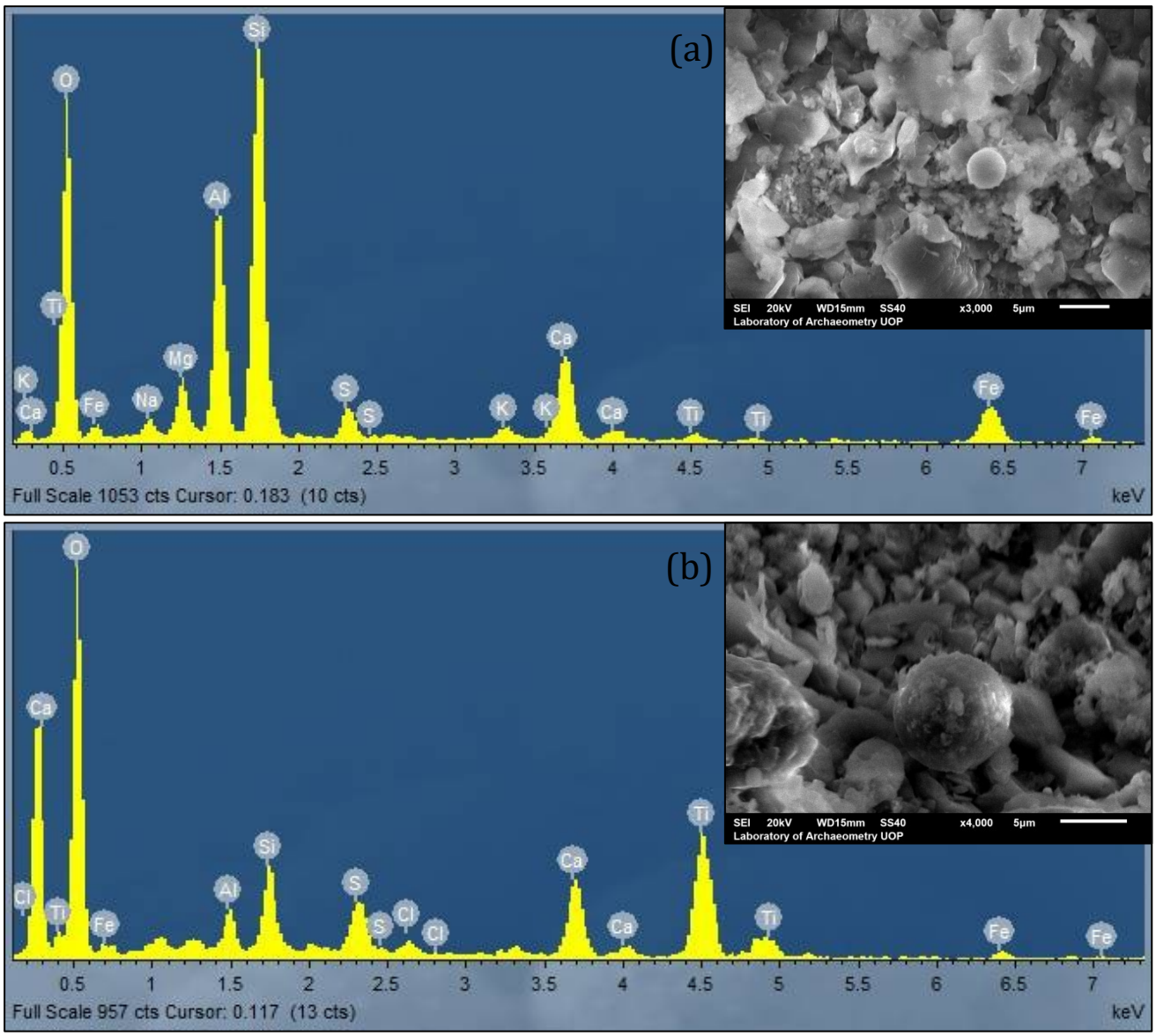

Fig. 55: SEM images and relative EDS spectra of (a) smooth and compact Al-Si particles and (b) Ti-rich particles in sample B4.

In sample B5, the crust shows a globular aspect, with a dense matrix and no visible macrocrystalline gypsum (Fig.56). There are three typologies of particles here as well: a) porous carbonaceous particles, rich in S and Ca (~ 10 μm), b) smooth and compact Fe-rich particles (~ 6 μm), and c) rough-dense Si-rich particles (~ 5 μm) (Fig. 57).

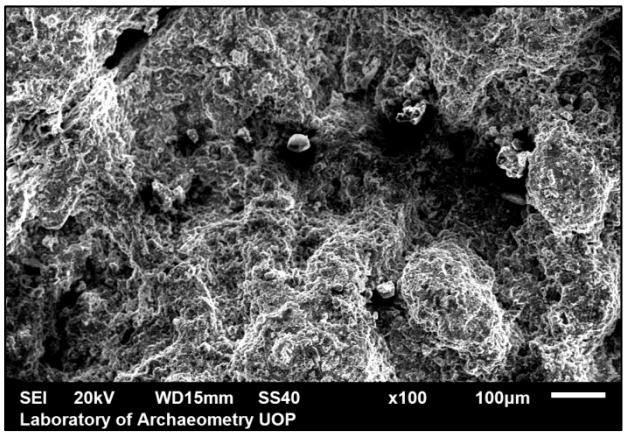

Fig. 56: SEM image of the crust surface of sample B5.

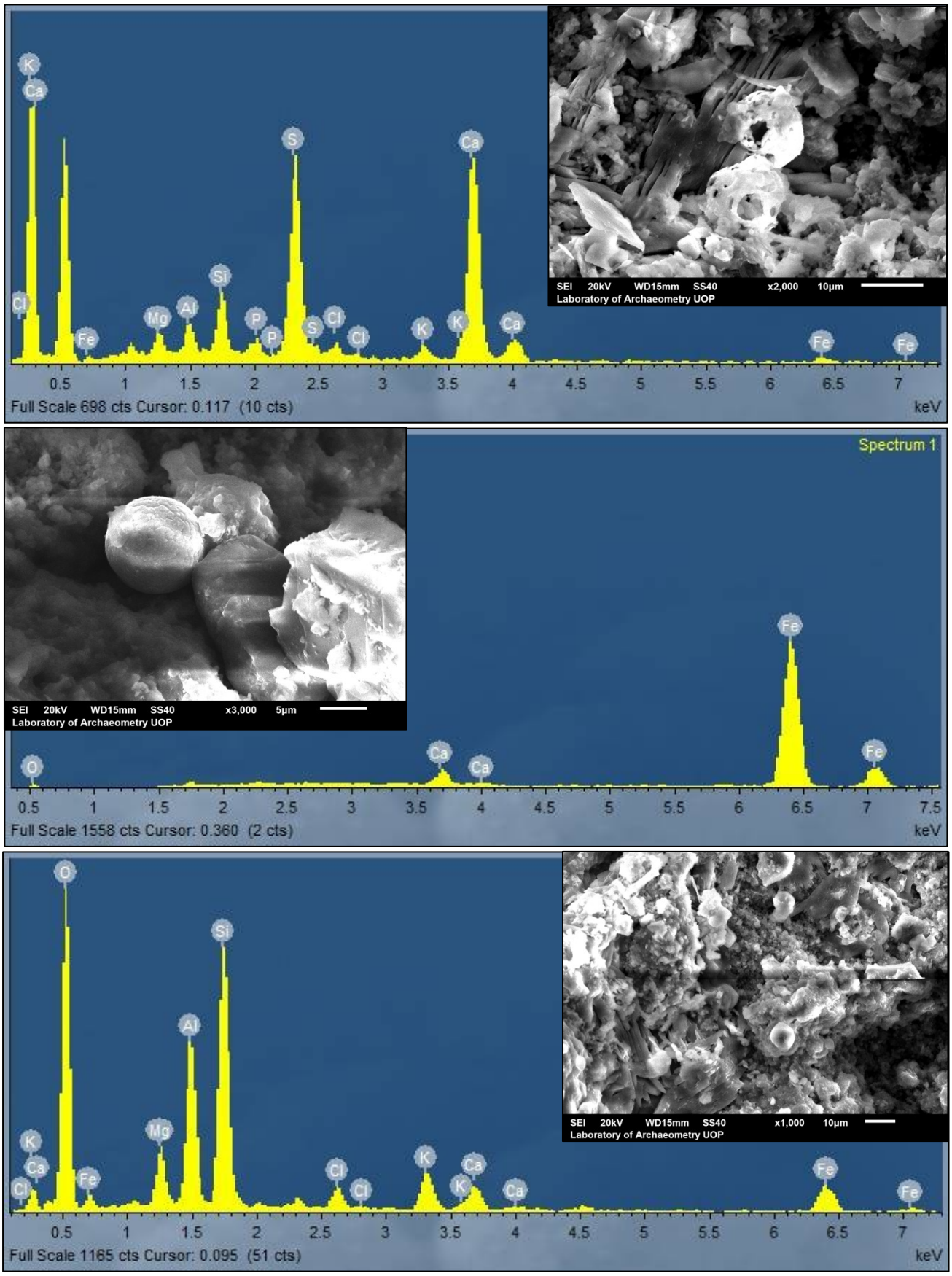

Fig. 57: SEM images and relative EDS spectra of (a) porous carbonaceous particles, rich in S and Ca (b) smooth and compact Fe-rich particles and (c) rough Si-rich particles.

4.e Micro X-ray Fluorescence

4.e.1 Quantitative data

As mentioned in the *Materials and methods* chapter, sample B1 provided sufficient material in order to enable powdering of the crust and pressing it into a tablet. The quantitative results for major and trace elements present in the crust, along with specifications for each measurement, are presented in Table 4.

Table 4: Major and trace element concentrations (in % or ppm, as indicated in the table) in sample B1, obtained by μ-XRF.

Element	FP-μXRF[1]	EM-μXRF[2]
S (%)	8.2	8.7
Cl (ppm)	999	-
K (ppm)	3685	-
Ca (%)	12.8	14.5
Ti (ppm)	452	-
Cr (ppm)	44.9	-
Mn (ppm)	99.7	-
Fe (ppm)	6027	-
Cu (ppm)	113	-
Zn (ppm)	190	-
Sr (ppm)	274	-
Zr (ppm)	199	-
Pb (ppm)	53.8	-

[1]Quantification through Fundamental Parameters approach.
[2]Quantification through empirical calibration with reference tablets.

As seen in the table above, the main constituents of the black crust are S (8.2%) and Ca (12.8%). Empirical calibration showed that the percentage of these two elements is not far from the measured quantities in FP-μXRF (8.7 and 14.5% respectively). There are elevated levels of K and Cl, the only elements apart from transition metals which are present in >1000 ppm or values close to 1000 ppm (3685 and 999 ppm respectively).

There are several transition metals present, in various concentrations. In order of abundance, they are: Fe (6027 ppm), Ti (452 ppm), Zr (199 ppm), Zn (190 ppm), Cu (113 pm), Mn (99.7 ppm) and Cr (44.9 ppm). Sr (274 ppm) and Pb (53.8 ppm) are also present. Comparison of this data with other sources is included in the *Discussion* chapter.

4.e.2 Line scans

Micro XRF provided the opportunity to perform line scans on a polished cross section of sample B1 and thus the ability to see the element distribution along the crust body. The line scans were performed on the external black crust of sample B1, due to the available material and the equipment settings. After preliminary scans, optimal measurement conditions were used in order to get as accurate results as possible, according to the area measured. The elements were measured at 50kV-600μA, with a 0.05mm step, and live time of 300s/step. The total number of measurements was 21. The results obtained for each element are presented in Fig. 58-59.

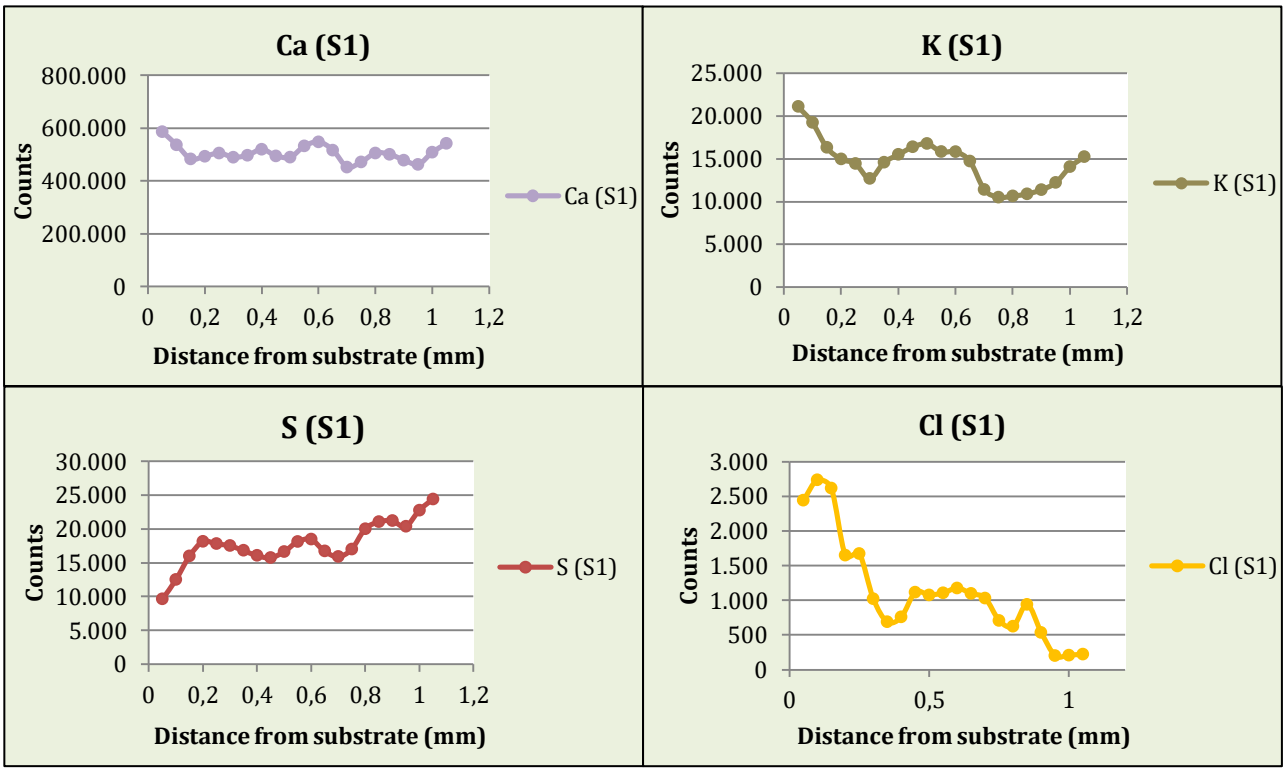

Fig. 58: Results of μ-XRF line scans for sample B1 (Ca, K, S and Cl).

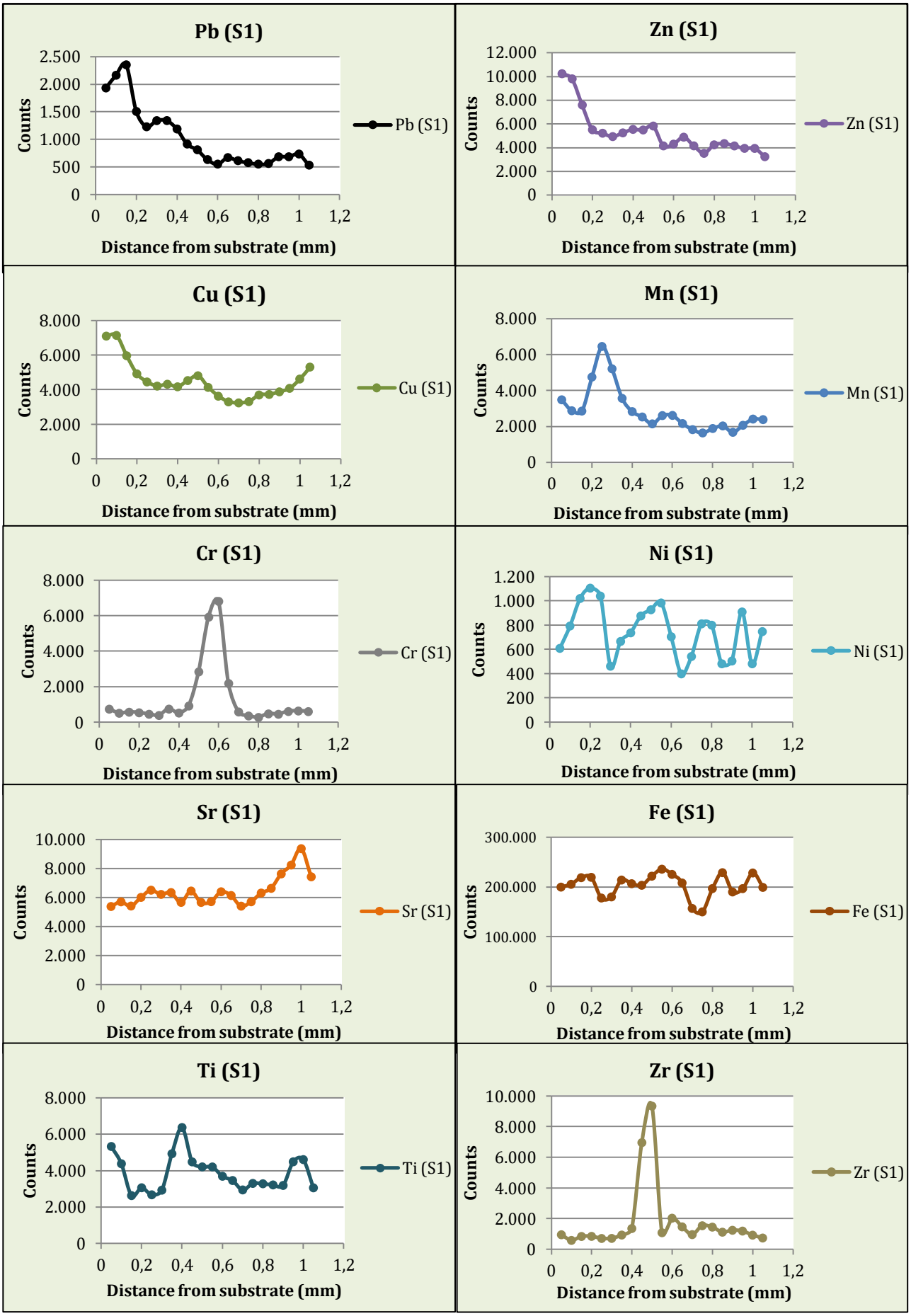

Fig. 59: Results of µ-XRF line scans for sample B1 (Pb, Zn, Cu, Mn, Cr, Ni, Sr, Fe, Ti and Zr).

As seen from the results for sample B1, the distribution of elements within the crust body is highly variable. Ca shows a homogeneous distribution along the crust profile, whereas S is increasing towards the crust surface. The distribution of heavy and transition metals is showing a great diversity. Pb, Zn and Mn levels are decreasing towards the surface of the crust. Fe has a rather homogeneous distribution, although small peaks can be observed. Cu is increased towards the substrate, steadily decreasing in the middle of the crust and then again slightly increasing towards the surface of the crust. Ni, Ti, Cr and Zr have a highly inhomogeneous distribution, with Ni and Ti showing multiple peaks and Cr and Zr being in the limit of detection almost throughout the entire crust profile and showing an intense peak in the middle of the crust. K rather follows the Cu pattern, with increased presence towards the substrate and the crust surface. Cl has high counts towards the substrate and steadily decreasing towards the crust surface. Finally, Sr is stable throughout the crust profile, with a slight increase towards the crust surface.

5. DISCUSSION

5.a Crust typology

After the completion of all the analytical techniques, interpretation and processing of the results is necessary, in order to extract possible conclusions. The typology of each crust sample was identified through macroscopic observations, optical and Scanning Electron Microscopy. All samples, except for sample B2, present the typical micromorphology and chemical composition of a black crust, with elevated values for S and Ca, denoting gypsum. The samples that provided sufficient material for a polished cross section (B1 and B4), gave further information about the specifics of the crust growth. As reported in the literature, a clear boundary between the substrate and the crust generally indicates that the crust is older than a crust that shows a gradual loss of continuity (Toniolo, et al., 2009; La Russa, et al., 2013).

The main constituents of the black crusts are S and Ca, indicating the presence of gypsum, as expected, except for sample B2, where an aluminosilicate, iron-rich patina is observed. This patina may indicate that an initial stage of black crusts includes the deposition of aluminosilicate and iron-rich particles mainly from mineral dust, before the growth of a black crust. This hypothesis is supported by the increased values of these elements in the inner layers of black crusts in samples B1 and B4.

The irregular case of samples B1 and B4, as mentioned earlier, includes the growth of two different crusts on both sides of exfoliated or partly detached pieces of marble substrate. According to all the information obtained by the optical microscopy observations, SEM images and SEM-EDS analyses, it is evident that in both cases the growth of a new crust on the internal surface of the samples occurred after the growth of the external crusts. A possible explanation is that small pieces of marble detached from the substrate, due to disintegration and increasing weight affected by their position on horizontal surfaces. The similarity in chemical composition with the crust of sample B2, determined as an initial stage of the growth of a black crust, supports this hypothesis.

Finally, the presence of lepidocrocite (γ-FeOOH) in both the crust and substrate of sample B1, as observed by means of μ-Raman spectroscopy, can be explained as a product of corrosion of iron. Lepidocrocite is a known component of rust in Cultural Heritage (Argo, 1981), and is proved to occur favorably in acidic conditions and the presence of sulphate anions (SO_4^{2-}), as is the case in black crusts (Montoya, et al., 2013).

5.b Enrichment factor analysis

The contribution of selected factors to each analyzed element was examined by using the enrichment factor (EF) analysis. In order to discriminate between the natural and anthropogenic sources of each element in the black crust of samples B1-B4, the elemental concentrations were compared to the substrate and the Earth's continental crust. The chemical composition of fresh Pentelic marble was used as a reference for sample B1 (Maravelaki-Kalaitzaki, 2005) and the SEM-EDS results from the unaltered substrate for sample B4, with Mg as the indicator element for sample B1 and Ti for sample B4, as they show small variations in substrates and black crusts. Accordingly, the abundance of major/trace elements in the continental crust, published by Taylor (1964), was used as a reference, with Al as the indicator element. The equations used for each element detected in the black crust (x) with respect to the substrate and the continental crust, are the following (Maravelaki-Kalaitzaki, 2005):

$$EF_{marble}\ (x) = \frac{\left({}^{x}/_{Mg\ or\ Ti}\right) crust}{\left({}^{x}/_{Mg\ or\ Ti}\right) marble}$$

$$EF_{con.\ crust}\ (x) = \frac{\left({}^{x}/_{Al}\right) crust}{\left({}^{x}/_{Al}\right) con.crust}$$

For the comparison with the substrate (Pentelic-Karystos marble), the major elements detected in SEM-EDS were used, due to lack of comparable trace element data for this material. For the comparison with the continental crust, both major and trace elements were used, based on the data provided by Taylor (1964), as proposed in other works, related to PM studies (Kanias, et al., 2004). The EFs for the major elements in samples B1-B4 were calculated for both layers of the black crust analyzed by means of SEM-EDS, as described in Chapter *4.d.2*. The EFs for the trace elements in sample B1 were calculated from the data provided by the elemental concentrations from μ-XRF, as described in Chapter 4.e.1. It should be noted that for sulfur, the quantitative data from μ-XRF were used, due to lack of SO_3 data for the continental crust. As a result, the EF for S with respect to the continental crust is presented in Table 6, together with the trace elements.

By convention, a threshold value of 3 was chosen, in order to distinguish between elements of the black crust and those of the substrate or the continental crust. This is an arbitrary value, but offers a threshold to determine the origin of an element, especially when there are multiple hints from supplementary analytical techniques.

In general, elements with EFs<3 indicate the substrate or the continental crust as their origin, respectively, and are termed non-enriched. Elements that show an EF>3 are considered to indicate that a significant proportion has a non-substrate or non-crustal material source (Moropoulou, et al., 1999). The results for both major and trace elements are presented in Tables 5 and 6, respectively.

Table 5: Enrichment factors for the major elements detected in the black crust of samples B1-B4 (BC1 = outer layer, BC2 = inner layer, EF values ≤ 3 highlighted in bold)

EF/Sample	Al_2O_3	SiO_2	P_2O_5	SO_3	Cl	K_2O	CaO	FeO	MgO
EF_{marble}/BC1	4.7	19.7	20.5	1.680,5	10	**2.5**	**0.1**	3.6	**1**
$EF_{con.crust}$/BC1	**1**	**1.2**	21.4	-	87.5	**1.3**	28.3	**0.9**	**1.6**
EF_{marble}/BC2	5.3	19.3	49.5	770	43	**3**	**0.1**	11.7	**1**
$EF_{con.crust}$/BC2	**1**	**1**	47.1	-	550	**1.4**	17.9	**2.5**	**1.4**
EF_{marble}/B4	12.4	34.8	6.9	48.9	3.9	7.3	**0.4**	22.3	18.1
$EF_{con.crust}$/B4	**1**	**0.9**	58.6	-	100	**1**	22.4	**1.2**	**2.1**

As seen in Table 5, there are groups of elements that show a rather clear origin. Ca clearly originates from the calcitic substrate. Regarding K and Mg, a substrate source can be explained for sample B1, whereas this is not the case for sample B4, probably due to the different type of marble. Al and Si are in good agreement with the composition of the Earth's crust, indicating mineral dust as their main source. Much the same could be said for Fe.

S, P and Cl show high enrichment with respect to both possible sources, therefore clearly originate from anthropogenic or other activities. It is generally accepted that Cl indicates marine spray as its main source (Zezza & Macri, 1995). Enrichment of P in the black crust could be linked to biological activity (Cnudde, et al., 2009).

Table 6: Enrichment factor the trace elements detected in the black crust of sample B1 (EF values ≤ 3 highlighted in bold)

	S	Ti	Cr	Mn	Fe	Cu	Zn	Sr	Zr	Pb
$EF_{con.\ crust}$	920	**0.25**	**1.7**	**0.3**	**0.4**	7.5	8	**3**	5	12.5

According to Table 6, the elements showing EF values lower than 3 are Ti, Cr, Mn, Fe and Sr. These elements are in good agreement with the crustal average values given by Taylor (1964), therefore can be attributed to mineral dust deposition. However, Cr, Mn and Fe can also be present in anthropogenic emissions and the SEM results for the detected particles reinforce this suggestion. Therefore such a source cannot be discarded. It is most probable that a proportion of these elements have multiple sources. S is again showing the highest values, clearly indicating an anthropogenic source. Cu, Zn, Zr and Pb originate from anthropogenic activities, as well, with characteristic high EF values. In general, emissions from diesel vehicle exhausts are characterized by higher concentrations of crustal elements, such as Al, Si, Fe, Ca and Mg, than anthropogenic elements, such as Cr, Cu, Mn, Ni, Pb, S, Ti and Zn. Sulfur emission is also the highest among non-metallic elements in gasoline combustion, indicating its origin (Wang, et al., 2003; Sharma, et al., 2005).

5.c Element distribution

The results from μ-XRF line scans can be further processed, in order to provide insight into possible correlations between specific elements. A Pearson's correlation matrix for the values reported for each element in the line scans, shows interesting features (Table 7). Values close to 1 mean that the element distribution is strongly correlated, whereas low or negative values show that the distribution of two elements is not correlated or even the opposite.

Table 7: Pearson's correlation matrix for the μ-XRF line scan values of sample B1 (colors are indicative of the correlation value)

	S	Cl	K	Ca	Ti	Cr	Mn	Fe	Ni	Cu	Zn	Sr	Zr	Pb
S	**1,00**													
Cl	**-0,76**	**1,00**												
K	**-0,62**	0,66	**1,00**											
Ca	**-0,28**	0,35	**0,71**	**1,00**										
Ti	**-0,35**	-0,06	**0,47**	0,38	**1,00**									
Cr	0,00	0,01	0,25	0,36	0,08	**1,00**								
Mn	-0,21	0,38	0,26	0,16	-0,14	-0,13	**1,00**							
Fe	0,15	0,10	0,41	0,41	0,30	**0,47**	-0,05	**1,00**						
Ni	-0,11	**0,31**	0,25	-0,07	-0,06	0,12	0,29	0,12	**1,00**					
Cu	-0,48	0,70	**0,81**	0,53	0,25	-0,19	0,26	0,24	0,26	**1,00**				
Zn	**-0,82**	**0,87**	0,79	0,47	0,32	-0,15	0,26	0,14	0,14	**0,85**	**1,00**			
Sr	**0,74**	**-0,63**	-0,32	-0,13	0,02	-0,15	-0,14	0,16	-0,25	-0,17	-0,48	**1,00**		
Zr	-0,13	-0,07	0,20	-0,14	0,18	0,21	-0,22	0,17	**0,22**	-0,04	0,02	-0,13	**1,00**	
Pb	**-0,65**	0,84	0,64	0,23	0,13	**-0,29**	**0,48**	0,10	0,28	0,80	**0,87**	-0,41	-0,19	**1,00**

As demonstrated in Table 7, there are some groups of elements that seem to share a common distribution along the crust profile. By highlighting the correlation values higher than 0.70 (with absolute correlation being 1.00), Ca, K and Ti share a common distribution, indicating that K and Ti most probably originate from the substrate, rather than mineral dust, as discussed earlier in the EFs analyses. Pb, Zn and Cu share a common distribution, with increased presence towards the substrate of the sample. These elements also indicated an anthropogenic source in the EF analysis. Pb and Zn are typical tracers for leaded gasoline combustion, which was used until about 20 years ago and show similar trends in other black crusts as well (Rodriguez-Navarro & Sebastian, 1996; Belfiore, et al., 2013).

As the innermost layers of the black crust supposedly represent older depositions, it could be assumed that Pb and Zn values correspond to the older use of leaded gasoline and the gradual change in vehicle engine fuel use during the past decades, as observed in other black crusts elsewhere (Török, et al., 2010; Belfiore, et al., 2013). This hypothesis is strongly related to the evident decrease of Pb content in the Athenian atmosphere, following the introduction of unleaded gasoline in the last 20 years (Scheff & Valiozis, 1990).

Cu shows an increased presence towards the surface of the crust, after a decline from the substrate. Cr and Ni also seem to be uncorrelated with the substrate, although their distribution does not help in categorizing them as recent deposits. This could be explained by the geochemical mobility of these elements, under specific conditions (McAlister, et al., 2008). These elements are typical tracers for oil combustion, diesel or gasoline and, considering their increased presence towards the surface of the crust, along with the notable decrease of Pb and Zn, it could be assumed that they denote the use of new engine fuels in the last decades (Rodriguez-Navarro & Sebastian, 1996; Geller, et al., 2006).

Fe distribution shows a correlation with substrate elements, such as Ca and K and insignificant variations along the black crust body. Therefore, it can be assumed that a significant proportion of this element derives from the dissolution of the marble. Other sources, such as mineral dust and anthropogenic emissions cannot be revealed by this method.

Finally, Cl distribution shows a great correlation with the metallic elements and specifically Zn, Pb, Cu and Mn. This correlation can be either explained by formation of salt crystals near the metallic content or by the halite (NaCl) crystals formation near the crust-substrate interface, as observed by means of SEM-EDS (Chapter 4.d.3). A hypothesis that these crystals could indicate elevated levels of marine aerosol in the past cannot be discarded, but there is not sufficient evidence to support it.

5.d Elemental composition

The Cu:Zn ratio in particulate matter has been successfully used in previous studies to determine a source of air pollution (Cadle, et al., 1999; Weckwerth, 2001; Valavanidis, et al., 2006). As demonstrated in the aforementioned literature, a ratio in the range of 0.1-0.5 is considered characteristic of emissions related to vehicle exhausts, whereas a ratio in the range of 0.7-1.5 is considered characteristic of emissions originating from industry.

The Cu:Zn ratio in the black crust of sample B1 is 0.59, indicating traffic as the main source of particulate matter pollution. Since these elements were determined to be of anthropogenic origin from the EF analysis, a suitable explanation for their origin can be given. In a study on particulate matter emissions in the centre of Athens in 2006 (Valavanidis, et al., 2006), the Cu:Zn ratio was determined as 0.2 for total suspended particulate (TSP), 0.5 for the coarse PM fraction ($PM_{10.1}$) and 0.38 for the fine PM fraction ($PM_{2.1}$).

The Cu:Zn ratio of sample B1 (0.59) is in good agreement with both the range given in the literature for traffic emissions (0.1-0.5) and the ratio given for the coarse PM fraction in the centre of Athens (0.5), where the Library of Hadrian is located. The common distribution of Cu and Zn, along with Pb (all related to vehicle exhaust emissions) in the Pearson's correlation matrix, reinforces this hypothesis. Other possible sources should always be taken into consideration for small proportions of these elements, as they are present in a solid black crust body and not in aerosol samples. However, even in this case, the ratio range is very characteristic to be ignored and it is evident that the majority of these elements derive from atmospheric deposition. Therefore, vehicular exhausts can be proposed as a major source of these elements for the particulate matter detected in the black crust matrix.

As discussed earlier, Mn presence in the black crust is probably due to mineral dust deposition, but an anthropogenic source cannot be excluded. Godelitsas et. al (2011) studied particulate matter from Athens and found many individual particles composed of Mn, possibly originating from gasoline additives, such as MCMT.

Fe, Cu, Zn and Pb comprise 90% of all metals present in Total Suspended Particulates (TSP) and both $PM_{2.5}$ and PM_{10} fractions in Athens (Valavanidis, et al., 2006). Much the same could be said for the black crusts (91.2% of all metals). Finally, a similar abundance and order of abundance of these elements is mentioned for TSP, PM fractions, vehicle exhausts and central heating in Athens and the black crusts in this study, giving another indication of their correlation (Fig. 60).

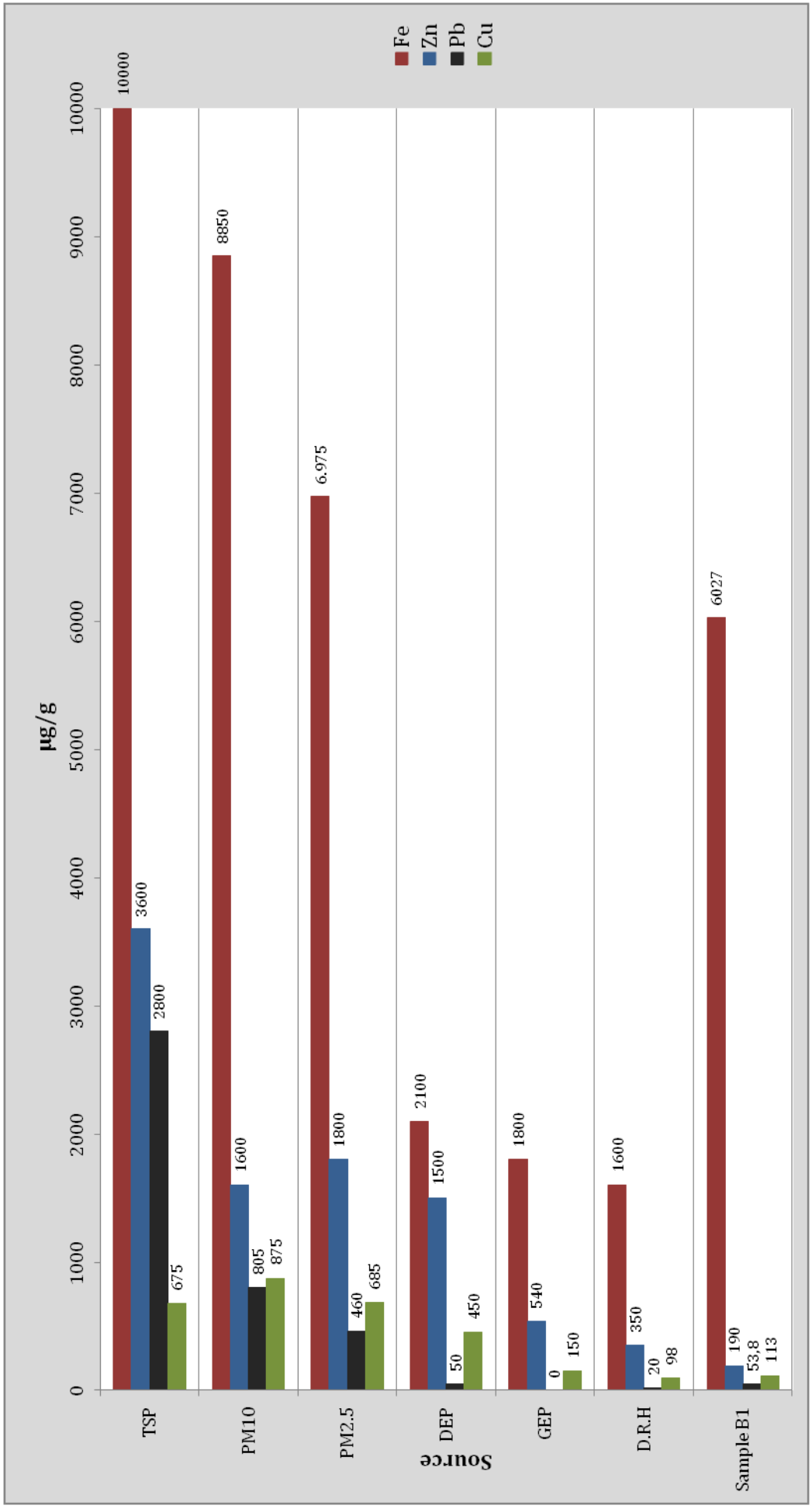

Fig. 60: Concentrations of various metals (Fe, Zn, Pb, Cu) in TSP, PM_{10}, $PM_{2.5}$ in Athens, gasoline exhausts (GEP), diesel exhausts (DEP), domestic residential heating (D.R.H.) (Valavanidis, et al., 2006) and sample B1

5.e Particulate matter characterization

In order to determine the source of the particles detected by means of SEM-EDS within the black crusts of the samples, a comparison with literature concerning PM in Greece has to be made. In particular, there are several studies on the size, morphology and elemental composition of PM measured in the centre of Athens that provide a sufficient reference (Valavanidis, et al., 2006; Karanasiou, et al., 2007; Godelitsas, et al., 2011). Additionally, there is sufficient material published including the characterization of specific aerosol particles found in Cultural Heritage damage layers or PM measurements, related to various pollution sources, such as vehicle exhausts, domestic heating and industrial emissions (Sabbioni & Zappia, 1992; Sabbioni, 1995; Rodriguez-Navarro & Sebastian, 1996; Labrada-Delgado, et al., 2012).

Regarding the Al-Si particles with a size of 5-8 μm, there is a clear correlation with soil dust from the surrounding area. The Al:Fe ratio has been used for the identification of the origin of particles in PM samples (Karanasiou, et al., 2007). The Al:Fe value for Al-Si particles in the coarse fraction in the present study (2.05) is in good agreement with the value reported for Athens soil (2.44) (Scheff & Valiozis, 1990), therefore indicating soil dust as their origin.

As far as the fine fraction of Al-Si particles is concerned, it has been demonstrated in numerous studies that they are of anthropogenic origin. In particular, Si-rich spherical particles with a smooth surface are fly ashes, mainly originating from coal and gas oil combustion, related to vehicular emissions (Sabbioni, 1995; Meszaros, et al., 1997; Bityukova, 2006; Ozga, et al., 2013; Perez-Monserrat, et al., 2016). The presence of such particles in the coarse fraction is merely due to the overgrown gypsum crystals, adding to the total size.

Regarding the carbonaceous particles, they can be divided into two categories: a) spherical-dense with a rough surface and b) spherical with a highly porous surface. The first category includes particles in both fractions ($PM_{2.5}$ and PM_{10}) and mainly originates from combustion sources and specifically diesel exhausts (Kjellstrom, et al., 2006; Labrada-Delgado, et al., 2012; Perez-Monserrat, et al., 2016). The second category is frequently found in both black crusts and particulate matter studies in Athens and is mainly associated with oil combustion (Sabbioni, 1995; Bonazza, et al., 2005; Godelitsas, et al., 2011; Perez-Monserrat, et al., 2016).

Fe-rich particles can be ascribed to several sources and need spot analyses including the detection of trace elements for a complete chemical characterization. However, candidate sources include distilled oil combustion in domestic heating (Sabbioni & Zappia, 1992) and coal combustion (Sabbioni, 1995; Perez-Monserrat, et al., 2016).

Furthermore, Ti-rich particles can be associated with coal combustion (Sabbioni, 1995) and industrial emissions (Maravelaki-Kalaitzaki, 2005), although the latter cannot be sufficiently supported, due to the lack of industrial fingerprints in the atmospheric depositions of the examined black crusts and the distance of the monument from such pollution sources.

Finally, particulate-bound polyaromatic hydrocarbons (PAHs) in the fine fraction of PM measurements in the centre of Athens were found to be associated mostly with diesel exhausts (Valavanidis, et al., 2006), as is the case with particles detected here. A complete categorization of the detected atmospheric particles, according to their size, type, micromorphological features and possible sources is provided in Table 8.

Table 8: Categorization of particles detected by means of SEM-EDS

($PM_{2.5}$ - PM_{10} fractions divided by dashed line)

Size (μm)	Type	Shape	Surface	Major elements	Source
1	Carbonaceous	Spherical	Rough	S, Ca	Diesel exhaust
2	Metallic	Spherical	Smooth	Si, Al	Coal-gas oil combustion (vehicular emissions)
3	Metallic	Spherical	Smooth	Si, S, Ca	Coal-gas oil combustion (vehicular emissions)
3	Metallic	Sub-spherical	Rough	Si, Al	Mineral dust
5	Metallic	Sub-spherical	Rough	Si, Al	Mineral dust
6	Carbonaceous	Spherical	Rough	S, Ca	Diesel exhaust
7	Metallic	Spherical	Smooth	Fe	Domestic heating/Coal combustion
7	Metallic	Spherical	Smooth	Ti, Si	Coal combustion
8	Metallic	Spherical	Smooth	Si, S, Ca	Coal-gas oil combustion
10	Carbonaceous	Sub-spherical	Porous	S, Ca	Oil combustion
10	Metallic	Spherical	Smooth	Ti	Coal combustion

5.f Effect of major pollutants

As discussed earlier in Chapter *2.d*, major pollutants (SO_2, NO_2, O_3 and PM) show a decrease in the last 25 years, as far as the surrounding area of the monument is concerned. The dramatic decrease in SO_2 concentrations should lead to a smaller rate of growth on the black crusts, as sulfur is the main component of the decay products. However, this is not the case, as sulfation is greatly affected by the presence of other major pollutants as well.

NO_2 concentrations may show a significant decrease throughout the last 25 years, but the concentration levels are still high and related to vehicular emissions of NO in urban traffic stations, such as the one located near the Library of Hadrian (Ministry of Environment and Energy, 2016). As NO_2 plays a catalytic role in the oxidation of SO_2 on the marble surface and the traffic in the surrounding area is still dense, its role in the formation of black crust is still important.

O_3 concentrations in the area also show a small overall decrease throughout the last decades, but tend to stabilize in the last 5 years. Generally, a decrease of NO_x emissions from traffic is followed by an increase of O_3 levels. As mentioned earlier in Chapter *2.c.1*, SO_2 oxidation with O_3 present in the atmosphere happens 1000 faster than with O_2. This possibly means that the oxidation rates of SO_2 related to the marble decay may be slower than in the past, but are still significant.

Furthermore, PM_{10} concentrations show a small decrease in the last decade, but tend to increase from 2012 onwards, mainly due to favorable conditions (decreased relative humidity) and biomass burning for domestic heating (Ministry of Environment and Energy, 2016). Additionally, PM measurements in Athens showed higher concentrations in winter, indicating the importance of local sources, mostly from vehicular exhausts (especially diesel) and diesel of central heating (Valavanidis, et al., 2006). These findings are in agreement with the types of particles detected in the black crust in this study, indicating domestic heating and diesel exhausts as their source.

The two major problems regarding air pollution in Athens in the most recent years is ozone and particulate matter (Valavanidis, et al., 2006). Currently, it seems that there is a stabilization of the growth rate of black crusts in the monument, but the accumulation of catalytic atmospheric particles and the high concentrations of ozone can set the basis for an even worse effect in the future, should the conditions change.

5.g Evaluation of methods

An evaluation of the methodology used is essential, in order to examine the level of success in covering the initial aims set for this study. As far as the characterization of the black crusts is concerned, Optical Microscopy, μ-Raman Spectroscopy and Scanning Electron Microscopy proved to be sufficient. The texture, color, grain size, micromorphological features and chemical and mineralogical composition of the crusts can be revealed by these methods and no further analytical procedure is needed, at least for the purposes of the present study. The only drawback concerning the chemical composition is the inability to detect and obtain quantitative data for carbon (C), which is always present in black crusts and could help in the characterization.

Regarding the identification of pollution sources, the presence of trace elements and especially heavy metals, which are not detected by means of SEM-EDS, could be revealed by μ-XRF. This analytical technique provided both quantitative data for these elements, along with the ability to see the element distribution along the crust body. This proved to be an important tool in understanding how these elements participate in the decay process and revealing their origin. Adding to this technique, the detection of atmospheric particles embedded in the black crusts by means of SEM-EDS also helped towards this direction, by providing images and their chemical composition. Another drawback of this technique was the inability to detect trace elements in the particles, which would help in a more complete characterization and correlation with other PM studies.

Overall, the methodology used is deemed sufficient, although a few alterations or additions (when possible) could improve the results and help in comparisons with similar works or between the samples. These alterations/additions include: a) larger samples in both volume and mass, in order to obtain polished cross sections, b) samples from monuments in different pollution backgrounds (e.g. industrial) and altitudes, c) the ability for isotopic analysis (especially for sulfur), measurement of elemental and organic carbon (EC-OC), and detection of trace elements in atmospheric particles.

6. CONCLUSIONS

After the completion of the analytical procedure, concluding remarks can be made, according to the initial aims, set in the beginning of this study. Regarding the characterization of the decay features present on the surface of the monument, it is evident that they consist of typical black crusts (samples B1, B3, B4 and B5) and an iron-rich aluminosilicate patina (sample B2), possibly acting as an initial stage of development of a black crust. The main constituents of the black crusts are gypsum and particles of variable chemical composition (carbonaceous and metallic). According to the specifics of each sample, such as the geometrical setting of the surface area, the presence or absence of water run-off/percolating water and the substrate material, there are small differences mainly in the morphology of the crusts. In general, it seems that thick dendritic black crusts grow on surfaces protected from water run-off, whereas thinner crusts with a laminar aspect grow on areas where the seasonal presence of percolating water is possible and are independent of the type of atmospheric pollutants accumulated on their surface. This is in agreement with the findings of several studies on black crusts on monuments in Greece (Moropoulou, et al., 1998; Maravelaki-Kalaitzaki, 2005) and elsewhere (Török, et al., 2010; Graue, et al., 2013).

The identification of pollution sources was possible by setting the methodology towards 3 main directions: a) the use of the chemical composition of the crusts in order to examine the origin of an element, b) the use of the element distribution along the crust in order to examine whether a chronological pattern in the deposition of pollutants could be revealed, and c) the characterization of individual embedded particles in order to identify their sources.

The results from the EF analysis and the Pearson's correlation matrix from the μ-XRF line-scans showed that there are groups of elements that have a specific origin and even correlate with each other. Elements such as Ca, K and Mg derive both from the substrate (Pentelic marble) and mineral dust depositions, although in sample B4, where a different substrate exists (Karystos marble), K and Mg seem to originate solely from mineral dust. Other elements, such as Al, Si, Fe, Ti, Cr and Mn seem to originate from mineral dust as well, although further investigation revealed other sources, at least for a small proportion of them. Chlorine presence is explained from the deposition of marine spray from the Saronic Gulf (Zezza & Macri, 1995) and phosphorus can be attributed to biological activity (Cnudde, et al., 2009). The clearly anthropogenic elements are S, Cu, Zn, and Pb.

The elements that show a good correlation in their distribution along the black crust body are: a) elements related to the substrate (Ca, K, Ti), b) transition and heavy metals with chlorine (Pb, Zn, Cu, Mn, Cl), and c) elements that show an irregular distribution due to their geochemical mobility or variation in possible sources (Fe, Cr, Ni). The distribution of Pb, Cu, Zn and Mn can be attributed to the gradual change of vehicle engine fuels and additives in the past decades (Rodriguez-Navarro & Sebastian, 1996; Geller, et al., 2006; Belfiore, et al., 2013).

A comparison of the proportion and order of abundance of characteristic elements (Fe, Pb, Cu, Zn) in the black crust with the PM in Athens showed a clear relation, regardless of the complexity of such a decay product. The Cu:Zn ratio also revealed that the atmospheric depositions on the black crusts mainly derive from vehicular emissions, again in agreement with the data provided for the surrounding area (Valavanidis, et al., 2006).

The characterization of the detected particles provided further information about their origin. The main typologies are: a) carbonaceous particles from diesel exhausts and domestic boilers, b) Si-rich particles from vehicular emissions and mineral dust, and c) metallic Ti-rich and Fe-rich particles from coal combustion and domestic heating, respectively. Therefore, it is evident that the main sources of particulate matter found in the crust are traffic (especially diesel exhausts) and domestic heating, again in agreement with the data provided for the centre of Athens (Valavanidis, et al., 2006; Godelitsas, et al., 2011; Ministry of Environment and Energy, 2016).

The effect of major pollutants is already evident in the presence of the black crusts and the future scenarios are not optimistic, as the accumulation of atmospheric particulates, along with the current trend on the concentration levels of ozone and nitrogen oxides and the relative humidity levels, can set favorable conditions for an even worse effect in the future, should the environmental conditions change. Taking into consideration the complex interrelation of the SO_2 oxidation rates with the concentrations of these pollutants and humidity, no safe predictions can be made on this matter. For example, a simple shift in the relative humidity levels, along with the presence of a large number of already accumulated catalytic particles, could lead to a fast growth of the black crusts and severe degradation of the already suffering surface of the monument.

There are specific drawbacks, concerning the analysis of black crusts and the identification of the pollution sources. The complexity of the material itself makes it difficult to accurately describe the aforementioned features, therefore multiple analytical techniques are required for a complete characterization.

The small size of the samples is a problem, as the (fair and justifiable) restrictions deriving from the historical significance of the monument complicate the analytical procedures even more.

Similar problems can cause the restrictions on the areas available for sampling, due to the lack of technological features (e.g. the scaffold used in this study).

A sampling strategy including obtaining crust fragments from multiple sides and heights of a single monument or from monuments with different pollution backgrounds (e.g. industry, traffic) could lead to a better understanding of the impact of air pollution in each case.

In order to better understand the mechanisms of growth of the black crusts and evaluate the level of involvement of each pollutant, further analytical techniques are necessary. Quantitative data for elemental and organic carbon can reveal the source of this element and be compared to other sources, especially in context with the evidently increased presence of smog from residential wood burning in the Athenian atmosphere in the last few years (Fourtziou, et al., 2016). Analysis of the sulfur and carbon isotopes could similarly help towards the same direction. A technique with the ability to detect and quantify trace elements in the detected particles would also add to a complete characterization and link to air pollution.

Overall, this study proposes a sufficient set of analytical techniques, with low cost, minimal damage to decay layers and no damage to original materials. It has been proved that black crusts can act as passive samplers and markers of historical changes in air pollution. There is a clear fingerprint of both the type and the chronological development of anthropogenic pollutants in a specific area. As unsightly as they might be, they are fine examples of the “memory effect” of nature on man-made changes in the environment. The correlation of a historically significant monument, its degradation products and environmental pollution is a proof of how science can find its place and give explanations in the immense complexity of natural and human-derived large-scale phenomena.

REFERENCES

Amoroso, G. G. & Fassina, V., 1983. *Stone Decay and Conservation.* Amsterdam: Elsevier Science Publishers B.V..

Argo, J., 1981. A Qualitative Test for Iron Corrosion Products. *Studies in Conservation, Vol. 26, No. 4*, November, pp. 140-142.

Assimakopoulos, D. et al., 1992. An experimental study of nighttime air-pollutant transport over complex terrain in Athens. *Atmospheric Environment, 26B*, pp. 59-71.

Belfiore, C. M. et al., 2013. Application of spectrometric analysis to the identification of pollution sources causing cultural heritage damage. *Environmental Science and Pollution Research, 20*, June, pp. 8848-8859.

Bingley, W., 1821. *Minerals.* Digital Edition ed. Harvard: Baldwin, Cradock, and Joy.

Bityukova, L., 2006. Air Pollution Effect on the Decay of Carbonate Building Stones in Old Town of Tallin. *Water Air and Soil Pollution, 172*, pp. 239-271.

Blatt, H. & Tracy, R., 1995. *Petrology, Second Edition: Igneous, Sedimentary and Metamorphic.* 2nd Edition ed. s.l.:W.H. Freeman.

Boatwright, M. T., 1983. Further Thoughts on Hadrianic Athens. *Hesperia: The Journal of the American School of Classical Studies at Athens, Vol. 52, No. 2*, April-June, pp. 173-176.

Bonazza, A., Sabbioni, C. & Ghedini, N., 2005. Quantitative data on carbon fractions in interpretation of black crusts and soiling on European built heritage. *Atmospheric Environment, 39*, pp. 2607-2618.

Brimblecombe, P., 2003. *The Effects of Air Pollution on the Built Environment.* London: Imperial College Press.

Brimblecombe, P., 2016. Past, Present and Future Damage to Materials and Building Surfaces in the Polluted Urban Environment. In: P. Brimblecombe, ed. *Urban Pollution and Changes to Materials and Building Surfaces.* London: Imperial College Press, pp. 1-18.

Cachier, H. et al., 2004. Aerosol characterization and sources in different European urban atmospheres: Paris, Seville, Florence and Milan. In: C. Saiz-Jimenez, ed. *Air Pollution and Cultural Heritage.* Sevilla: CRC Press, pp. 3-14.

Cadle, S. H., Mulawa, P. A. & Hunsanger, E. C., 1999. Composition of light-duty motor vehicle exhaust particulate matter in the Denver, Colorado area. *Environmental Science and Technology, 33*, pp. 2328-2339.

Camuffo, D., Del Monte, M., Sabbioni, C. & Vittori, O., 1982. Wetting, deterioration and visual features of stone surfaces in an urban area. *Atmospheric Environment, 16*, pp. 2253-2259.

Cassar, J., 2016. The Historic and Archaeological Heritage: Pollution and Non-Urban Sites. In: P. Brimblecombe, ed. *Urban Pollution and Changes to Materials and Building Surfaces.* London: Imperial College Press, pp. 255-290.

Castro, K. et al., 2005. On-line FT-Raman and dispersive Raman spectra database of artists' materials (e-VISART database). *Analytical and Bioanalytical Chemistry, 382*, June, pp. 248-258.

Charola, A. E. & Ware, R., 2002. Acid deposition and the deterioration of stone: a brief review of a broad topic. In: G. S. Siegesmund, A. Vollbrecht & T. Weiss, eds. *Natural stone, weathering phenomena, conservation strategies and case studies.* London: Geological Society, pp. 393-406.

Choremi-Spetsieri, A., 1995. The Library of Hadrian at Athens: Recent Finds. *Ostraka, 4*, pp. 137-147.

Cnudde, V. et al., 2009. Multi-disciplinary characterisations of a sandstone surface crust. *Science of the Total Environment, Vol. 407*, pp. 5417-5427.

Dermentzopoulos, T. et al., 1988. Building stones of ancient monuments in Attica; an outline. In: P. G. Marinos & G. C. Koukis, eds. *The Engineering Geology of Ancient Works, Monuments and Historical Sites.* Brookfield: A.A. Balkema Publishers, pp. 619-629.

Dinsmoor, W. B., 1950. *The Architecture of Ancient Greece: An Account of Its Historic Development.* New York: Biblo & Tannen Publishers.

Fant, C., 1995. Augustus and the city of marble. In: M. Schvoerer, ed. *Archéomatériaux: Mabres et autres roches.* Bordeaux: Recherche en Physique Appliquée à l'Archéologie, Presses Universitaires de Bordeaux, pp. 277-280.

Fellenberg, G., 2000. *The chemistry of pollution.* Chichester: Wiley.

Fourtziou, L. et al., 2016. Multi-tracer approach to characterize domestic wood burning in Athens (Greece) during wintertime. *Atmospheric Environment*.

Fronteau, G. et al., 2010. Black-crust growth and interaction with underlying limestone microfacies. In: R. Přikryl & A. Török, eds. *Natural Stone Resources for Historical Monuments.* London: Geological Society.

Gaffney, J. S. & Marley, N. A., 2009. The impacts of combustion emissions on air quality and climate-from coal to biofuels and beyond. *Atmospheric Environment, 43*, pp. 23-36.

Garrison, E., 2003. *Techniques in Archaeological Geology.* New York: Springer Science & Business Media.

Geller, M. D. et al., 2006. Physicochemical and redox characteristics of particulate matter (PM) emitted from gasoline and diesel passenger cars. *Atmospheric Environment, 40*, pp. 6988-7004.

Ghedini, N. et al., 2011. Atmospheric aerosol monitoring as a strategy for the preventive conservation of urban monumental heritage: The Florence Baptistery. *Atmospheric Environment, 45 (33)*, October, pp. 5979-5987.

Godelitsas, A. et al., 2011. A microscopic and Synchrotron-based characterization of urban particulate matter (PM10-PM2.5 and PM2.5) from Athens atmosphere, Greece. *Nuclear Instruments and Methods in Physics Research B, 269*, April, pp. 3077-3081.

Graindor, P., 1935. Athènes sous Hadrien. *Revue belge de philologie et d'histoire, Vol. 14, 3*, pp. 926-931.

Graue, B. et al., 2013. The effect of air pollution on stone decay: the decay of the Drachenfels trachyte in industrial, urban, and rural environments-a case study of the Cologne, Altenberg and Xanten cathedrals. *Environmental Earth Sciences, 69*, pp. 1095-1124.

Greek Ministry of Culture, 2012. *http://odysseus.culture.gr/.* [Online]
Available at: http://odysseus.culture.gr/h/3/eh351.jsp?obj_id=2370
[Accessed 16 June 2016].

Hellenic Statistical Authority, 2011. *Ανακοίνωση προσωρινών αποτελεσμάτων Απογραφής Πληθυσμού 2011,* Peiraeus: s.n.

ICOMOS, 1965. *International Charter for the Conservation and Restoration of Monuments and Sites.* Venice, ICOMOS.

ICOMOS, 2008. *Illustrated glossary on stone deterioration patterns.* s.l.:ICOMOS.

Ivaskova, M., Koteš, P. & Brodnan, M., 2015. Air Pollution as an Important Factor in Construction Materials Deterioration in Slovak Republic. *Procedia Engineering, 108*, December, pp. 131-138.

Jameson, R., 1816. *System of Mineralogy.* 2nd Edition ed. Lausanne: A. Constable & Company.

Janhäll, S. et al., 2009. Evolution of urban aerosol during winter temperature inversion episodes. *Atmospheric Environment, 40*, September, pp. 5355-5366.

Johansson, I. G., Lindquist, O. & Mangio, R. E., 1988. Corrosion of calcareous stones in humid air containing SO2 and NO2. *Durability of Building Materials, 5*, April, pp. 439-449.

Kalabokas, P. D., Viras, L. G. & Repapis, C. C., 1999. Analysis of the 11-year record (1987-1997) of air pollution measurements in Athens, Greece. Part I: Primary air pollutants. *Global Nest International Journal, Vol 1, No 3*, pp. 157-167.

Kanias, G. D., Viras, L. G. & Grimanis, A. P., 2004. Source identification of trace elements emitted into Athens atmosphere-Relation between trace elements and tropospheric ozone. *Journal of Rdioanalytical and Nuclear Chemistry, Vol. 260, No. 3*, pp. 509-518.

Karanasiou, A. A., Sitaras, I. E., Siskos, P. A. & Eleftheriadis, K., 2007. Size distribution and sources of trace metals and n-alkanes in the Athens urban aerosol during summer. *Atmospheric Environment, 41*, pp. 2368-2381.

Kassomenos, P., Kotroni, V. & Kallos, G., 1995. Analysis of climatological and air quality observations from Greater Athens Area. *Atmospheric Environment, Vol. 29, No. 24*, pp. 3671-3688.

Kjellstrom, T. et al., 2006. Air and Water Pollution: Burden and Strategies for Control. In: D. T. Jamison, J. G. Breman, A. R. Measham & e. al., eds. *Disease Control Priorities in Developing Countries.* New York: Oxford University Press.

La Russa, M. F. et al., 2013. Geochemical study of black crusts as a diagnostic tool in cultural heritage. *Applied Physics A*, 27 August, pp. 1151-1162.

Labrada-Delgado, G. et al., 2012. Chemical and morphological characterization of PM2.5 collected during MILAGRO campaign using scanning electron microscopy. *Atmospheric Pollution Research, 3*, pp. 289-300.

Laskaridis, K. & Patronis, M., 2009. «Καρυστία Λίθος» Ένα διαχρονικό δομικό υλικό. *Ελληνική Γεώσφαιρα, 3, 6*, April, pp. 5-12.

Maravelaki-Kalaitzaki, P., 2005. Black crusts and patinas on Pentelic marble from the Parthenon and Erechtheum (Acropolis, Athens): characterization and origin. *Analytica Chimica Acta, 532*, pp. 187-198.

Maravelaki-Kalaitzaki, P. & Biscontin, G., 1999. Origin, characteristics and morphology of weathering crusts on Istria stone in Venice. *Atmospheric Environment, 33*, pp. 1699-1709.

Mastrapas, A., 1999. *Μνημειακή τοπογραφία της αρχαίας Αθήνας.* Athens: Kardamitsa Publications.

McAlister, J. J., Smitha, B. J. & Torok, A., 2008. Transition metals and water-soluble ions in deposits on a building and their potential catalysis of stone decay. *Atmospheric Environment, 42*, pp. 7657-7668.

Meszaros, E. et al., 1997. Size distributions of inorganic and organic species in the atmospheric aerosol in Hungary. *Journal of Aerosol Science, 28*, pp. 1163-1175.

Ministry of Environment and Energy, 2016. *Annual report on atmospheric pollution,* Athens: Ministry of Environment and Energy.

Montoya, P., Echavarria, A. & Calderon, J. A., 2013. Influence of Anion and pH on the Electrochemical Co-Deposition and Transformation of Iron Oxy-Hydroxide. *International Journal of Electrochemical Science*, 20 October, pp. 12566-12579.

Morillas, H. et al., 2016. Study of particulate matter from Primary/Secondary Marine Aerosol and anthropogenic sources collected by a self-made passive sampler for the evaluation of the dry deposition impact on built heritage. *Science of the Total Environment, 550*, pp. 285-296.

Moropoulou, A. et al., 1998. Origin and growth of weathering crusts on ancient marbles in industrial atmosphere. *Atmospheric environment, Vol. 32, No. 6*, March, pp. 967-982.

Moropoulou, A., Bisbikou, K., Torfs, K. & Van Grieken, R., 1999. Risk analysis for the protection of cultural heritage from industrial pollution. *Transactions on the Built Environment, vol. 39*, pp. 475-484.

Nathanson, J. A., 2015. *www.britannica.com.* [Online]
Available at: https://www.britannica.com/science/pollution-environment
[Accessed 14 September 2016].

Omidvarborna, H., Kumar, A. & Kim, D.-S., 2015. Recent studies on soot modeling for diesel combustion. *Renewable and Sustainable Energy Reviews, Vol. 48*, August, pp. 635-647.

Ozga, I. et al., 2013. Pollution impact on the ancient ramparts of the Moroccan city Salé. *Journal of Cultural Heritage, 145*, June, pp. S25-S33.

Ozga, I. et al., 2011. Diagnosis of surface damage induced by air pollution on 20th-century concrete buildings. *Atmospheric Environment, 45*, pp. 4986-4995.

Ozga, I. et al., 2014. Assessment of air pollutant sources in the deposit on monuments by multivariate analysis. *Science of the Total Environment, 490*, June, pp. 776-784.

Pausanias, 1918. *Pausanias Description of Greece, Books 1-2.* Revised ed. Edition ed. Cambridge: Harvard University press.

Penkett, S. A., Jones, B. M. R., Brice, K. A. & Eggleton, A. E. J., 1979. The importance of atmospheric ozone and hydrogen peroxide in oxidizing sulphur dioxide in cloud and rainwater. *Atmospheric Environment, 13*, pp. 123-137.

people.duke.edu, 2016. *people.duke.edu.* [Online]
Available at: http://people.duke.edu/~wj25/uc_web_site/libraries/hadrian.html
[Accessed 27 July 2016].

Pérez-Alonso, M., Castro, K. & Madariaga, J. M., 2006. Vibrational Spectroscopic Techniques for the Analysis of Artefacts with Historical, Artistic and Archaeological Value. *Current Analytical Chemistry, 2*, pp. 89-100.

Perez-Monserrat, E. M., Varas-Muriel, M. J., De Buergo, M. A. & Fort, R., 2016. Black Layers of Decay and Color Patterns on Heritage Limestone as Markers of Environmental Change. *Geosciences, 6, 4*, 7 January.

Prieto-Taboada, N. et al., 2013. Buildings as repositories of hazardous pollutants of anthropogenic origin. *Journal of Hazardous Materials, 248-249*, 11 January, pp. 451-460.

Raddato, C., 2014. *commons.wikimedia.org.* [Online]
Available at:
https://commons.wikimedia.org/wiki/File:The_west_facade_in_Pentelic_marble_with_columns_of_Karystos_marble_of_the_Library_of_Hadrian,_Athens_(13890230681).jpg
[Accessed 27 July 2016].

Rodriguez-Navarro, C. & Sebastian, E., 1996. Role of particulate matter from vehicle exhaust on porous building stones (limestone) sulfation. *The Science of the Total Environment, 187*, pp. 79-91.

Sabbioni, C., 1995. Contribution of atmospheric deposition to the formation of damage layers. *The Science of the Total Environment, 167*, pp. 49-55.

Sabbioni, C., Ghedini, N. & Bonazza, A., 2003. Organic anions in damage layers on monuments and buildings. *Atmospheric Environment, 37, 9-10*, March, pp. 1261-1269.

Sabbioni, C. & Zappia, G., 1992. Characterization of particles emitted by domestic heating units fueled by distilled oil. *Atmospheric Environment, Vol. 26A, No. 18*, pp. 3297-3304.

Sanjurjo-Sánchez, J. & Alves, C., 2011. Decay effects of pollutants on stony materials in the built environment. *Environmental Chemistry Letters, 10*, 28 December, pp. 131-143.

Schaffer, R., 1932. *The weathering of natural building stones,* London: Department of Scientific and Industrial Building Research, His Majesty's Stationary Office, Report no. 18.

Scheff, P. A. & Valiozis, C., 1990. Characterization and source identification of respirable particulate matter in Athens, Greece. *Atmospheric Environment, Vol. 24A, No. 1*, pp. 203-211.

Sharma, M., Kumar Agarwal, A. & Bharathi, K. V. I., 2005. Characterization of exhaust particulates from diesel engine. *Atmospheric environment, 39*, pp. 3023-3028.

Shear Jr, T., 1981. Athens: From City-State to Provincial Town. *Hesperia, 50*, pp. 356-377.

Sisson, M., 1929. The Stoa of Hadrian at Athens. *papers of the British School at Rome, Vol. 11*, pp. 50-72.

Smith, B., Gomez-Heras, M. & McCabe, S., 2008. Understanding the decay of stone-built cultural heritage. *Progress in Physical Geography, 32 (4)*, pp. 439-461.

Sourlas, D., 2011. *www.tap.gr.* [Online]
Available at:
http://www.tap.gr/tapadb/components/com_jshopping/files/demo_products/004_BAD_Bibliothiki_Adranou_W.pdf
[Accessed 28 May 2016].

Steiger, M., 2003. Salts and crusts. In: P. Brimblecombe, ed. *The Effects of Air Pollution on the Built Environment.* London: Imperial College Press, pp. 133-181.

Stewart, J. & Revett, N., 2007. *The Antiquities of Athens: Measured and Delineated by James Stuart and Nicholas Revett, Painters and Architects.* 1st Edition ed. Princeton: Princeton Architectural Press.

Taylor, S. R., 1964. Abundance of chemical elements in the continental crust: a new table. *Geochimica et Cosmochimica Acta, Vol. 28*, pp. 1273-1285.

Toniolo, L., Zerbi, C. M. & Bugini, R., 2009. Black layers on historical architecture. *Environmental Science and Pollution Research, 16*, pp. 218-226.

Török, A., Licha, T., Simon, K. & Siegesmund, S., 2010. Urban and rural limestone weathering; the contribution of dust to black crust formation. *Environmental Earth Sciences*, 16 September.

Tung, A., 2001. *"The City the Gods Besieged". Preserving the World's Great Cities: The Destruction and Renewal of the Historic Metropolis..* New York: Three Rivers Press.

United Nations, 2003. *Geology and Mineral Resources of Timor-Leste.* s.l.:United Nations Publications.

Valavanidis, A. et al., 2006. Characterization of atmospheric particulates, particle-bound transition metals and polycyclic aromatic hydrocarbons of urban air in the centre of Athens (Greece). *Chemosphere, 65*, pp. 760-768.

Vrekoussis, M. et al., 2013. Economic crisis detected from space: Air quality observations over Athens/Greece. *Geophysical Research Letters, Vol. 40*, pp. 458-463.

Wang, Y. F. et al., 2003. Emissions of fuel metals content from a diesel vehicle engine. *Atmospheric Environment, 37*, pp. 4637-4643.

Weckwerth, G., 2001. Verification of traffic emitted aerosol components in the ambient air of Cologne (Germany). *Atmospheric Environment, 3*, pp. 5525-5536.

Zezza, F. & Macri, F., 1995. Marine aerosol and stone decay. *Science of the Total Environment, Vol. 167, 1-3*, May, pp. 123-143.

ΕΜΕΚΑ, 2011. *Οι περιβαλλοντικές, οικονομικές και κοινωνικές επιπτώσεις της κλιματικής αλλαγής στην Ελλάδα,* Athens: Bank of Greece.

APPENDICES

APPENDIX I

1.1 Sampling spots

Sample B1

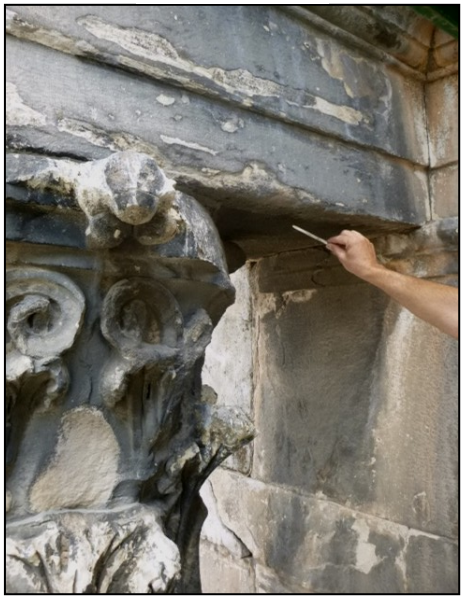

Sample B2

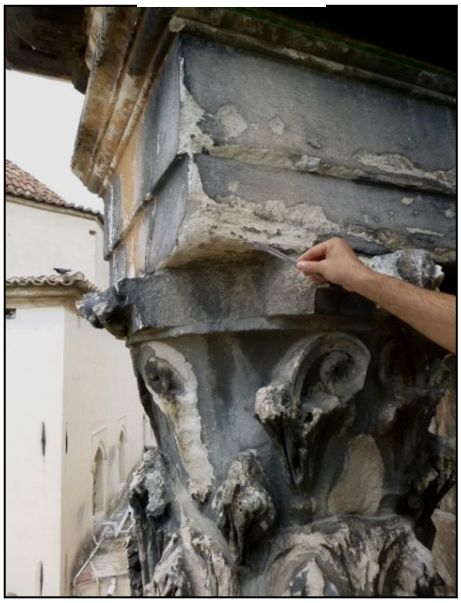

Sample B3

Sample B4

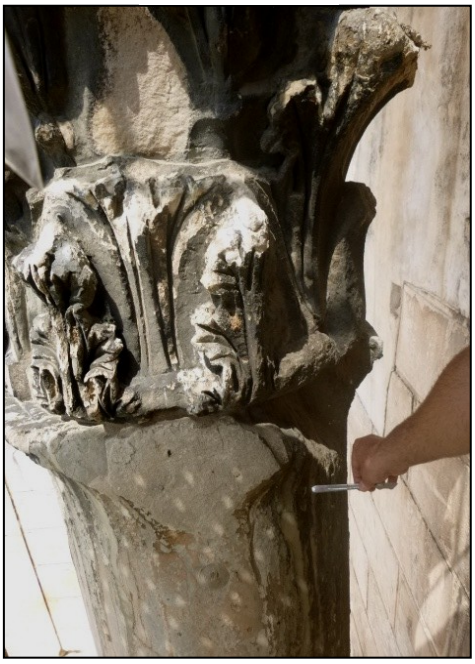

Sample B5

1.2 Images of the samples

Sample B1

Substrate

Surface

Sample B2

Surface

Sample B3

Substrate

Surface

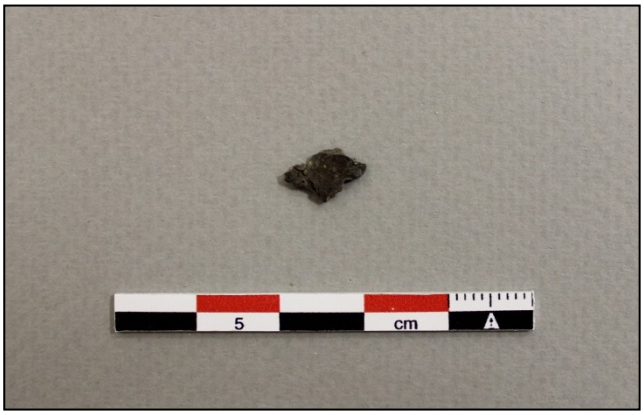

Sample B4

Substrate

Surface

Sample B5

Surface

1.3 Optical microscopy images

Sample B1

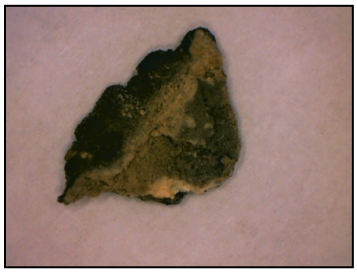
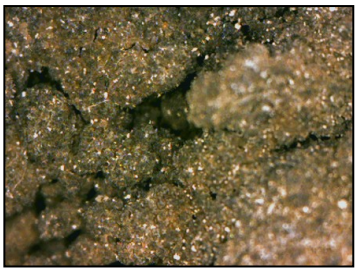


Sample B2

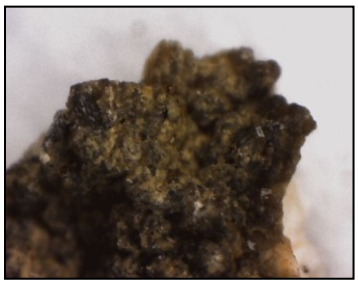
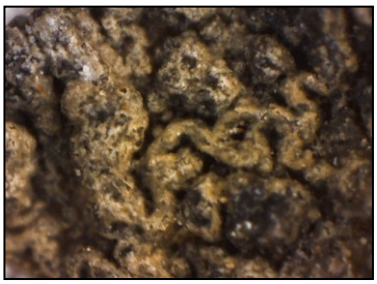


Sample B3

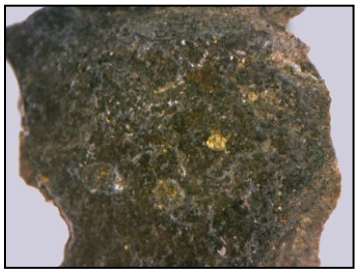
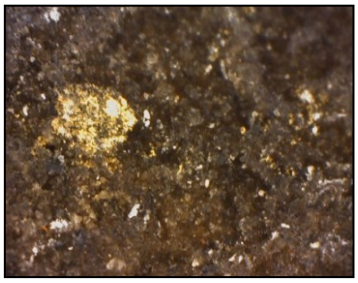


Sample B4


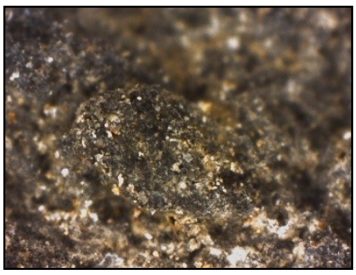


Sample B5

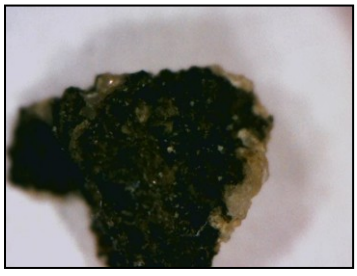
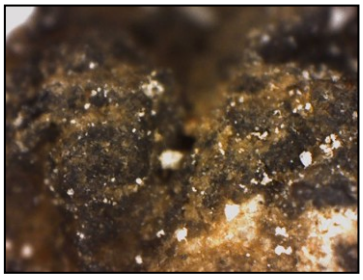
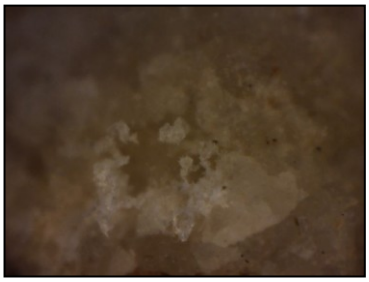

APPENDIX II

2.1 SEM spectra for bulk measurements

Sample B1

Crust

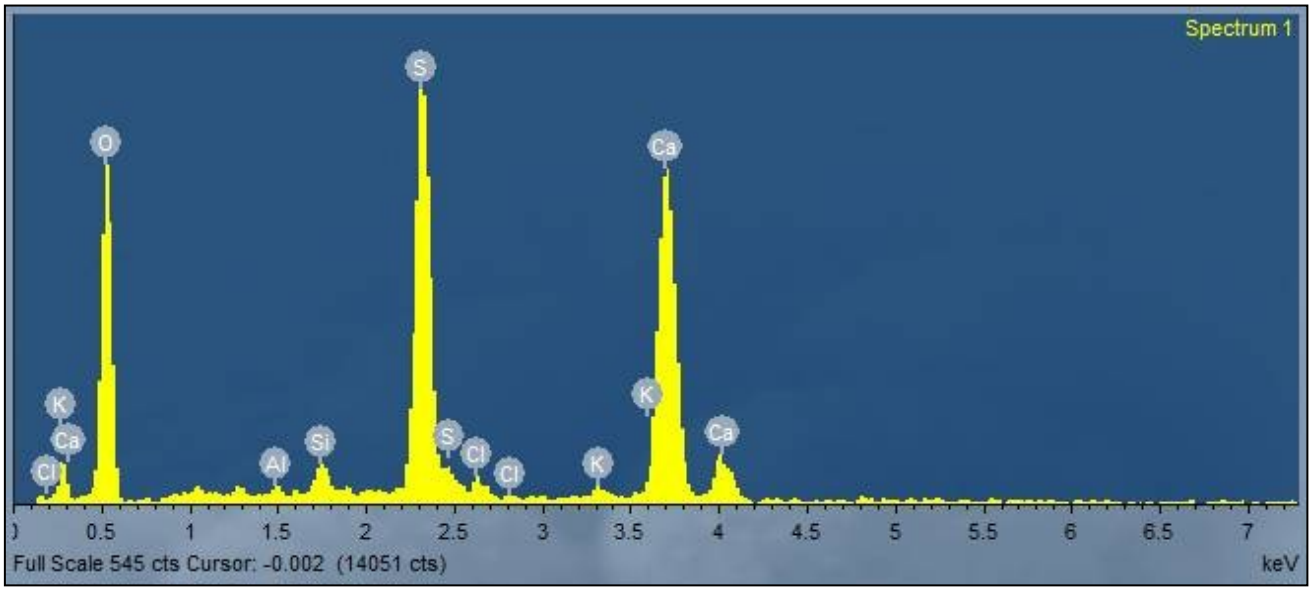

Substrate

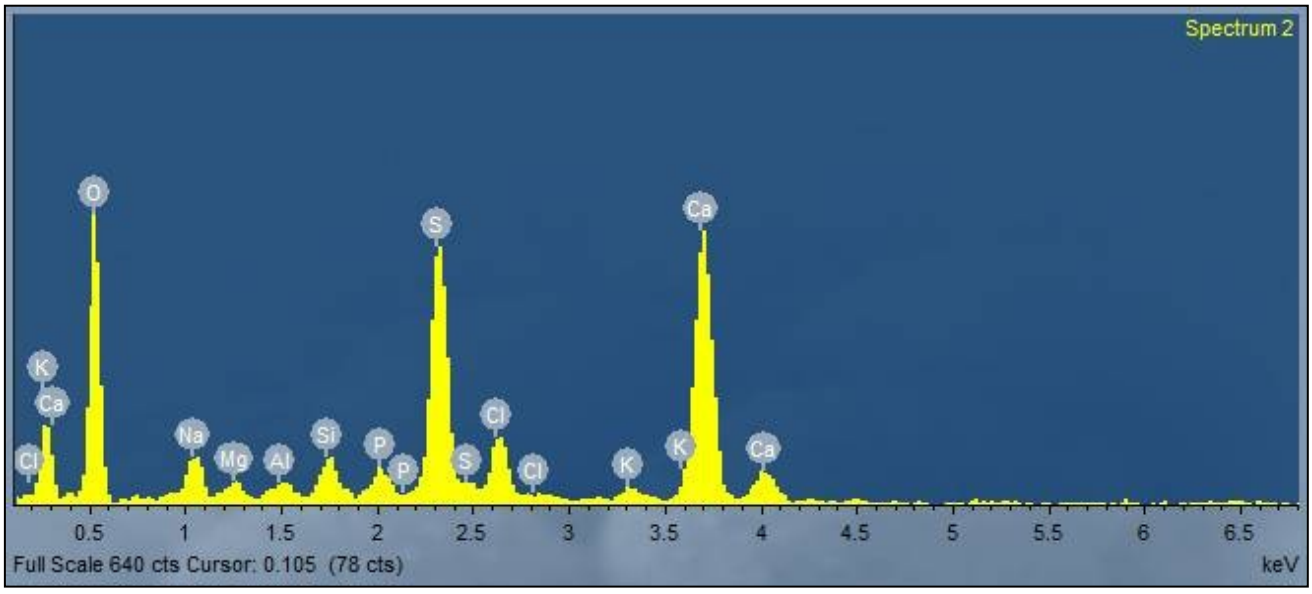

Sample B2

Crust

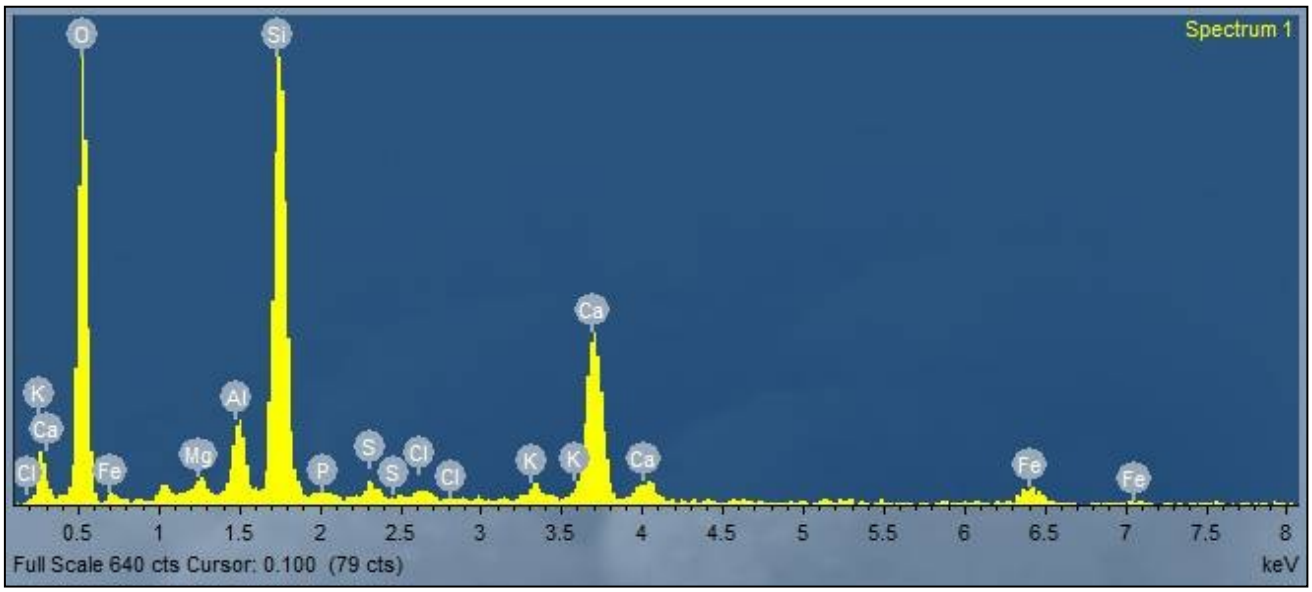

Substrate

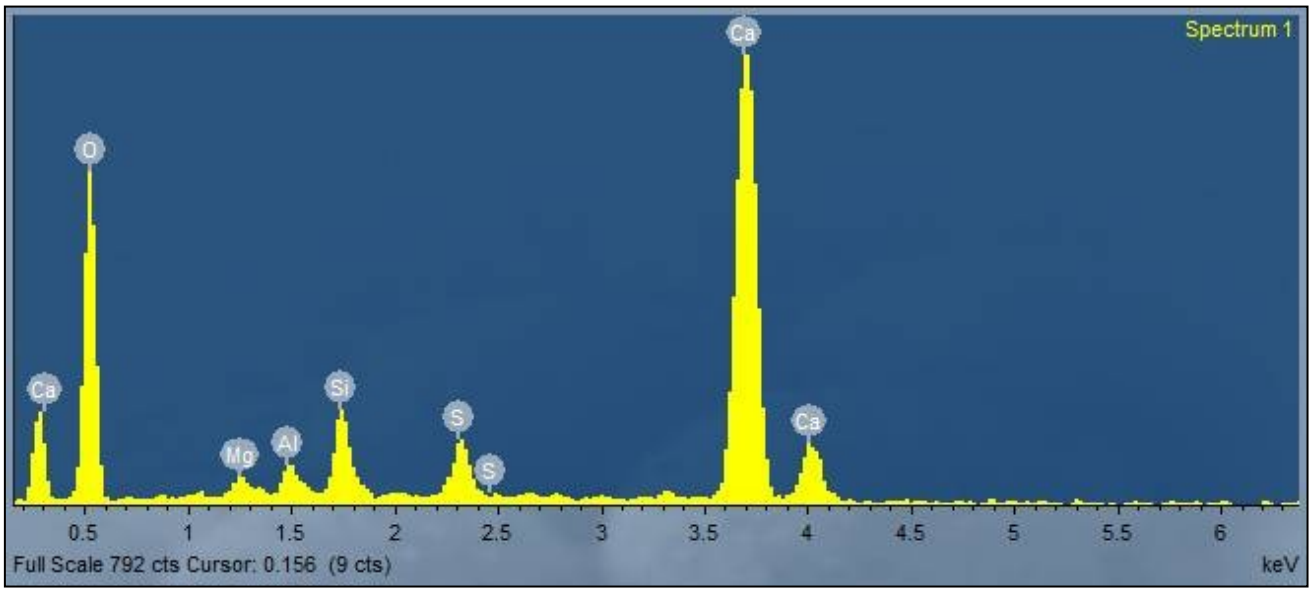

Sample B3

Crust

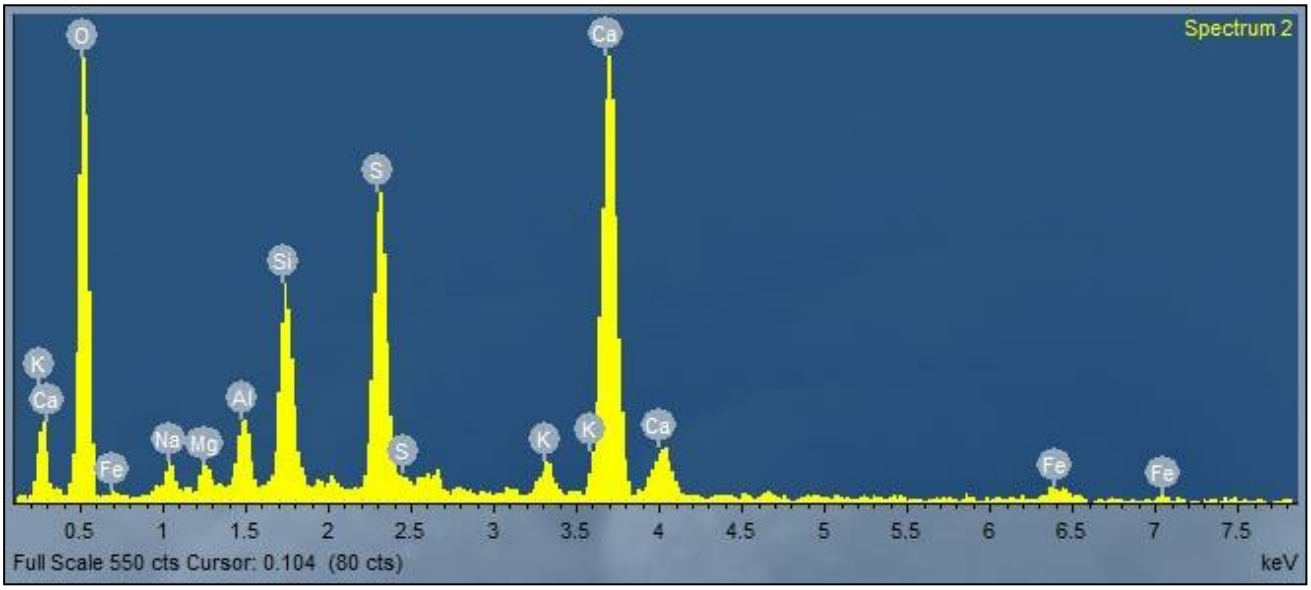

Substrate

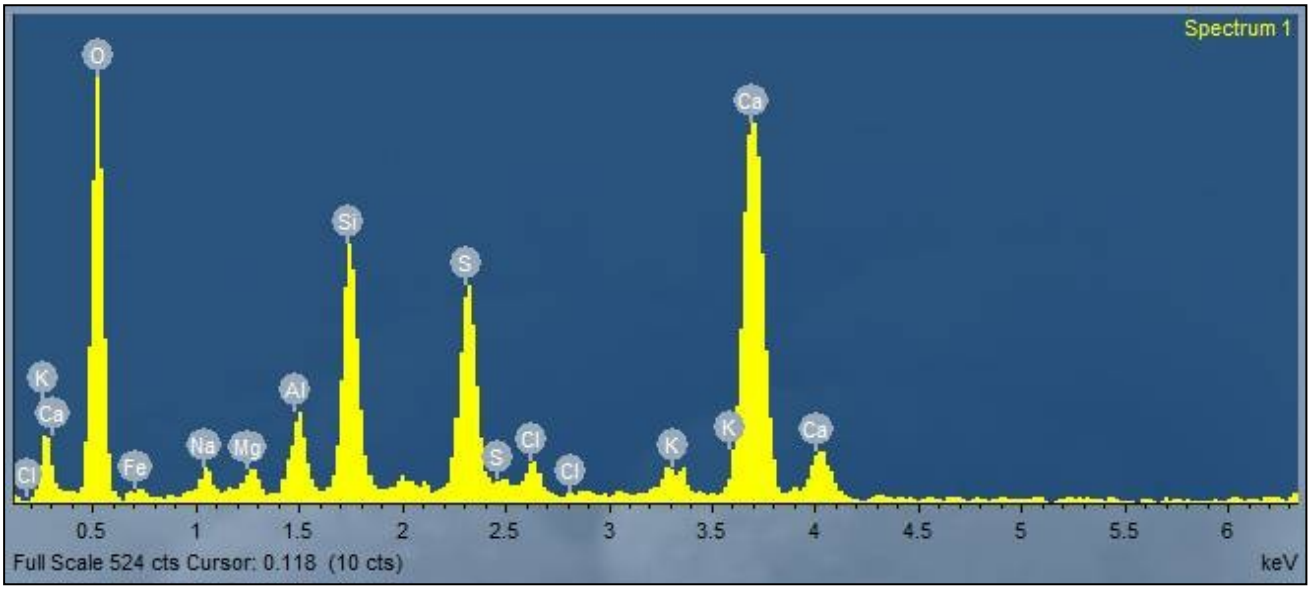

Sample B4

Crust

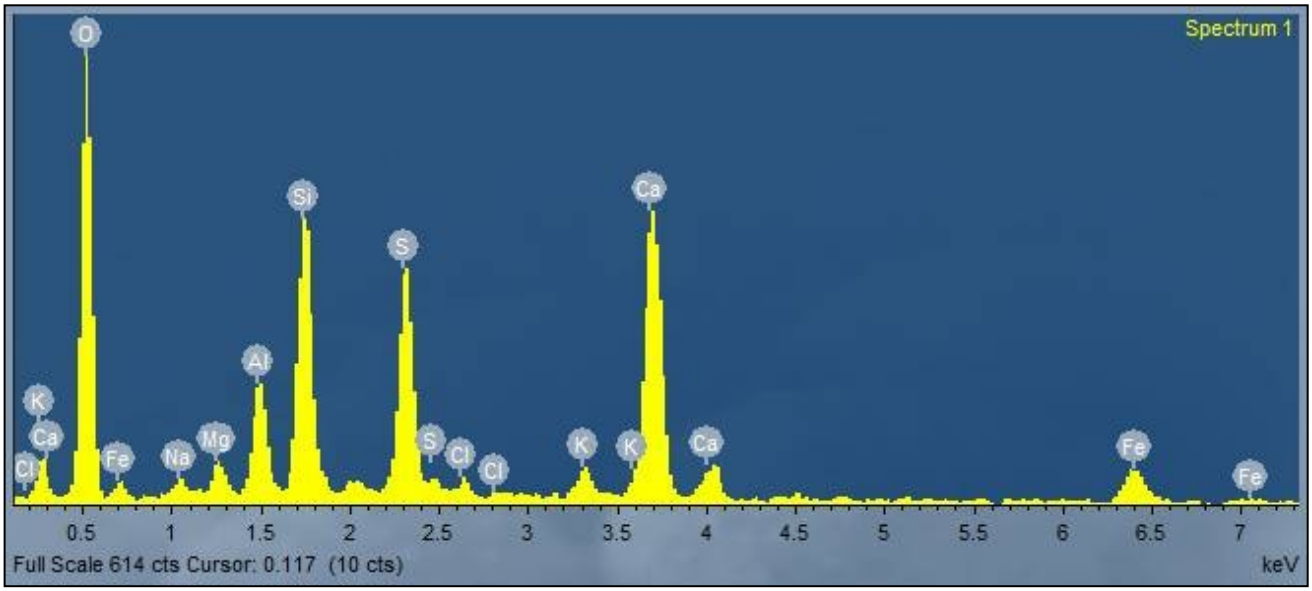

Substrate

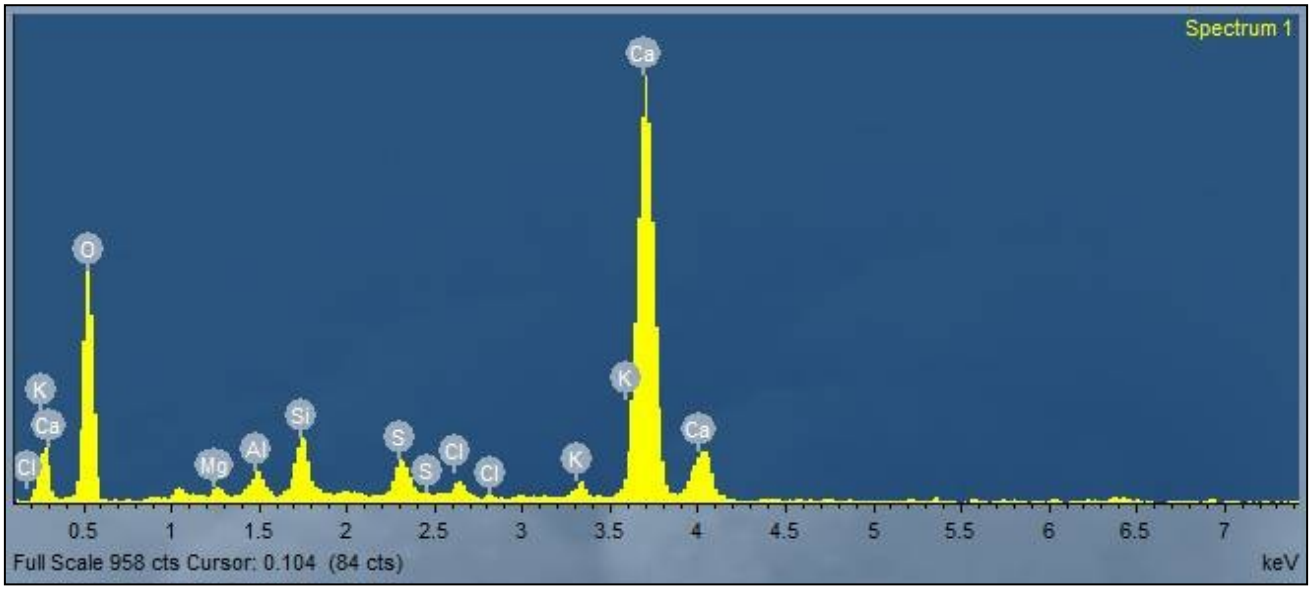

Sample B5

Crust

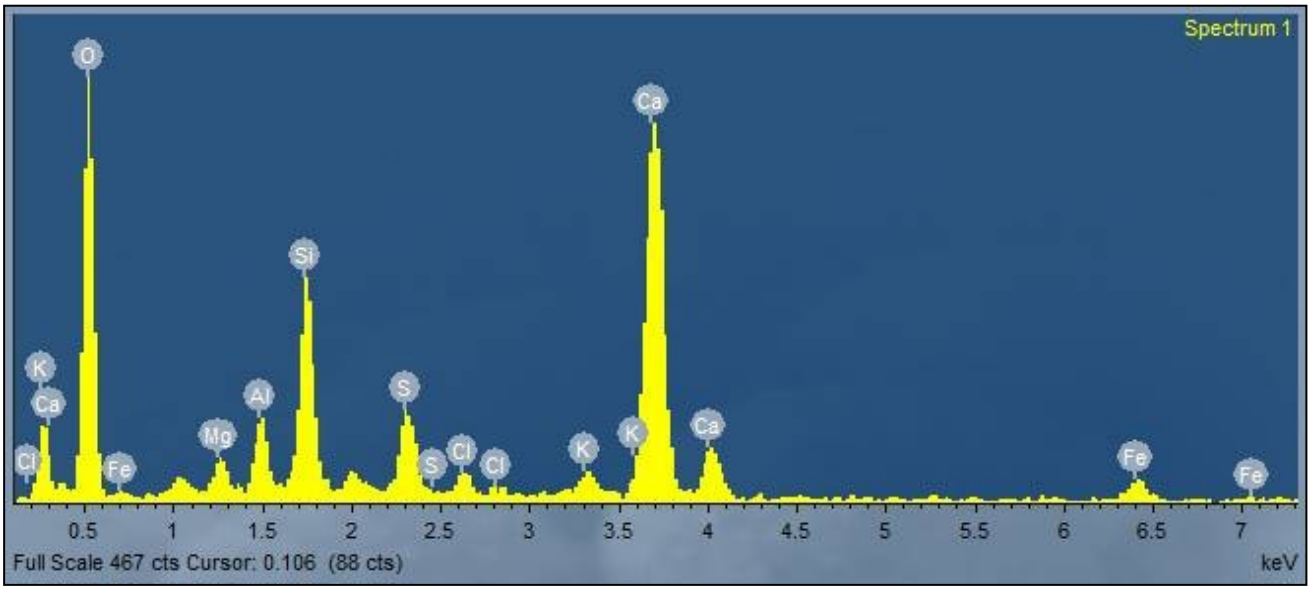

Substrate